

Dispersion relationship of phononic generalized beams

Mario Lázaro^{a,b,*}, Richard Wiltshaw^b, Richard V. Craster^b, Vicent Romero-García^a

^a*Instituto Universitario de Matemática Pura y Aplicada, Universitat Politècnica de València, 46022 (Spain)*

^b*Department of Mathematics, Imperial College London, London, SW7 2AZ, UK*

Abstract

In this work, we present a comprehensive method for determining the dispersion relation in one-dimensional waveguides, applicable to a wide range of structures, regardless of their specific characteristics. This general framework employs a unified mathematical model, referred to as *generalized beams*, where varying types of waveguides and scatterers are incorporated by adjusting certain parameters. The generalized beam consists of a host waveguide, which is a homogeneous elastic structure with physical properties represented in matrix form. The model also accounts for an arbitrary set of scatterers within the unit cell, including resonators (discrete and continuous), small material inclusions, or variations in cross-sectional area. Based on general assumptions, we develop a matrix-based algorithm utilizing the plane wave expansion method to derive the solution. Additionally, we propose an iterative procedure that provides analytical expressions for the first- and second-order terms, particularly useful in the context of weak scattering. The convergence conditions of the method are rigorously defined. The approach's effectiveness is demonstrated through several numerical examples, highlighting its versatility in different waveguide configurations and scattering scenarios.

Keywords:

elastic waveguides, dispersion relation, weak scattering, iterative method, one-dimensional phononic crystals

1. Introduction

Phononic metamaterials have gained significant importance in recent decades due to their ability to control the propagation of low-frequency waves through structured media containing arrays of resonators that operate at single frequencies [1] for multiple frequencies [2–6]. The design paradigm of metamaterials is widely adopted across various domains of wave physics to create subwavelength devices by leveraging these resonances, such as in photonics [7, 8] phononics [9–12]. Examples include energy harvesting [13–16] and seismic protection devices [17–21]. Furthermore, new designs incorporating attached Rayleigh beams explore the coupling between longitudinal and flexural motion components to manage wave responses [22–24]. For flexural waves in plates, the introduction of point oscillators necessitates the use of multiple scattering methods combined with the plane wave expansion method [6, 25–29].

The study of high-contrast elastic solids and heterogeneous materials, particularly focusing on their inherent resonances and properties after perturbation, is highly relevant in the fields of experimental modal analysis and structural health monitoring [30]. Analytical approximations combined with finite element methods have been suggested for analyzing vibrating structures for assessing transmission and reflection caused by the introduction of multiple oscillators [31–34] as well as for studying dynamical behavior of elastic waveguides with properties that vary along their length [35–40].

*Corresponding author. Tel +34 963877000 (Ext. 76732)
Email address: malana@mes.upv.es (Mario Lázaro)

Additionally, for the mathematical modeling of impedance contrast due to cracks, internal elastic springs in conjunction with spectral element method [41–44] or specially developed finite elements [45] have been developed. In the realm of nanomaterial mechanics, theories relying on material distinctions have been suggested for analyzing how structures with numerous cracks spread across their length behave and how they affect the modal characteristics. This applies to both flexural waves (in nanobeams) [46] and longitudinal waves (in nanorods) [47].

Traditionally, analytical procedures for obtaining the dispersion relation in one-dimensional homogeneous media have been presented separately in the literature [48–50], starting with classical media such as the bar (longitudinal and torsional waves) and the Euler-Bernoulli beam (flexural waves) to continue with modified models (higher-order rod or beam theories). The intricacy grows as the number of variables increases, rendering the analytical solutions for the differential equation of time-varying motion difficult to handle, particularly when factoring in localized disruptions within the medium like attached objects or variations in material and cross-sectional properties. Hence, it's beneficial to present the constitutive equations in a first-order format [51], as it simplifies the expression of continuity conditions across progressively expanding degrees of freedom (such as displacement, rotation, force, moments, etc.) into a matrix. Consequently, the objective of this paper is to construct a comprehensive analytical framework in matrix notation aimed at deriving the dispersion relationship of one-dimensional elastic waveguides accommodating an arbitrary number of scatterers (be they resonators, inclusions, or heterogeneities), all while assuming a flexible number of degrees of freedom in the modeling process.

In this paper, we present an analytical method to determine the dispersion relation in one-dimensional waveguides containing an arbitrary number of scatterers, which can take the form of point resonators, small material inclusions, and/or changes in cross-sectional area. We introduce a unified mathematical framework that applies to any type of scatterer, allowing for a generalized approach. This mathematical model is called the *generalized beam* to highlight the fact a vast number of both elastic structures and scatterers can be considered under the same mathematical framework. The problem is solved using the plane wave expansion technique, and an iterative procedure is developed to express the dispersion relation as a perturbation of the host-beam wavemodes. This approach, based on the weak scattering assumption, provides analytical solutions that accurately predict wave propagation. We also rigorously establish the numerical convergence criteria for the iterative method. The theoretical findings are validated through three numerical examples: (i) an Euler-Bernoulli beam with point spring-mass resonators, (ii) waveguides with small inclusions affecting both longitudinal and flexural waves, and (iii) a Timoshenko beam with continuous resonators (embedded beams).

2. The generalized beam

In this work, we are mainly interested on investigating the dispersion relations of an elastic one-dimensional structure with an arrangement of N perturbations or scatterers distributed along each unit cell of length L . Before outlining the methodology proposed in this paper, it is important to first present the foundational analytical model used to describe the homogeneous elastic medium, i.e., the system without any perturbations. This background will provide essential context for understanding the effects of scatterers on wave propagation in the waveguide.

One-dimensional models enable us to represent the displacement pattern of any cross-section using generalized parameters that solely rely on the longitudinal position x . By employing Hamilton's principle in conjunction with cross-sectional kinematic assumptions, a series of partial differential equations emerge in space-time dimensions (x, t) , expressed in terms of m kinematic parameters and m generalized forces, denoted as $\mathbf{v}(x, t)$ and $\mathbf{F}(x, t)$, respectively. Generally, all system parameters can be encapsulated into a

column vector, referred to as the state-vector $\mathbf{u}(x, t)$ of dimension $2m$, structured as follows:

$$\mathbf{u}(x, t) = \begin{Bmatrix} \mathbf{v}(x, t) \\ \mathbf{F}(x, t) \end{Bmatrix}. \quad (1)$$

Assuming that the waveguide is homogeneous and harmonic response, i.e. that $\mathbf{u}(x, t) = \mathbf{u}(x)e^{i\omega t}$ for radian-frequency ω , the space-time partial differential equations governing the constitutive relations can be expressed as

$$\frac{d\mathbf{u}}{dx} = \mathbf{A} \mathbf{u} + \mathbf{q}(x), \quad (2)$$

where the matrix \mathbf{A} is a $(2m) \times (2m)$ matrix with frequency dependent terms containing the stiffness, mass and inertia parameters of the waveguide. The vector $\mathbf{q}(x)$ represents the distributed external loads associated with any generalized forces acting over the waveguide, and hence $\mathbf{q}(x)$ only has entries in the last m terms. It is interesting to visualize some examples of application and for that in Table 1 the state-vector, the external forces and the matrix \mathbf{A} are listed for several particular cases including classical and higher-order models for longitudinal, flexural and torsional waves, including an example of coupled flexural-torsional waves.

Model	$\mathbf{u}(x)$	$\mathbf{q}(x)$	Matrix \mathbf{A}
Longitudinal (classical rod) $2m = 2$	$\begin{Bmatrix} u \\ N_x \end{Bmatrix}$	$\begin{Bmatrix} 0 \\ -q_x \end{Bmatrix}$	$\begin{bmatrix} 0 & 1/EA \\ -\rho A\omega^2 & 0 \end{bmatrix}$
Longitudinal (Love's rod) $2m = 2$	$\begin{Bmatrix} u \\ N_x \end{Bmatrix}$	$\begin{Bmatrix} 0 \\ -q_x \end{Bmatrix}$	$\begin{bmatrix} 0 & 1/(EA - \rho I_x v^2 \omega^2) \\ -\rho A\omega^2 & 0 \end{bmatrix}$
Torsional (Saint-Venant) $2m = 2$	$\begin{Bmatrix} \theta_x \\ T_x \end{Bmatrix}$	$\begin{Bmatrix} 0 \\ -m_x \end{Bmatrix}$	$\begin{bmatrix} 0 & 1/GJ \\ -\rho I_x \omega^2 & 0 \end{bmatrix}$
Torsional (Open thin-walled Vlasov beams) $2m = 4$	$\begin{Bmatrix} \theta_x \\ \varphi \\ T_x \\ M_w \end{Bmatrix}$	$\begin{Bmatrix} 0 \\ 0 \\ -m_x \\ 0 \end{Bmatrix}$	$\begin{bmatrix} 0 & 1 & 0 & 0 \\ 0 & 0 & 0 & 1/EI_w \\ -\rho I_x \omega^2 & 0 & 0 & 0 \\ 0 & \rho I_w \omega^2 - GJ & -1 & 0 \end{bmatrix}$
Flexural (Euler-Bernoulli) $2m = 4$	$\begin{Bmatrix} w \\ \theta_y \\ V_z \\ M_y \end{Bmatrix}$	$\begin{Bmatrix} 0 \\ 0 \\ -q_z \\ -m_y \end{Bmatrix}$	$\begin{bmatrix} 0 & 1 & 0 & 0 \\ 0 & 0 & 0 & 1/EI_y \\ -\rho A\omega^2 & 0 & 0 & 0 \\ 0 & 0 & -1 & 0 \end{bmatrix}$
Flexural (Timoshenko) $2m = 4$	$\begin{Bmatrix} w \\ \theta_y \\ V_z \\ M_y \end{Bmatrix}$	$\begin{Bmatrix} 0 \\ 0 \\ -q_z \\ -m_y \end{Bmatrix}$	$\begin{bmatrix} 0 & 1 & 1/GA_z & 0 \\ 0 & 0 & 0 & 1/EI_y \\ -\rho A\omega^2 & 0 & 0 & 0 \\ 0 & -\rho I_y \omega^2 & -1 & 0 \end{bmatrix}$
Flexural-torsional y -symmetry (Timoshenko, Saint-Venant) $2m = 6$	$\begin{Bmatrix} w \\ \theta_y \\ \theta_x \\ V_z \\ M_y \\ T_x \end{Bmatrix}$	$\begin{Bmatrix} 0 \\ 0 \\ 0 \\ -q_z \\ -m_y \\ -m_x \end{Bmatrix}$	$\begin{bmatrix} 0 & 1 & 0 & 1/GA_z & 0 & 0 \\ 0 & 0 & 0 & 0 & 1/EI_y & 0 \\ 0 & 0 & 0 & 0 & 0 & 1/GJ \\ -\rho A\omega^2 & 0 & -\rho Ay_G \omega^2 & 0 & 0 & 0 \\ 0 & -\rho I_y \omega^2 & 0 & -1 & 0 & 0 \\ -\rho Ay_G \omega^2 & 0 & -\rho I_x \omega^2 & 0 & 0 & 0 \end{bmatrix}$
Flexural-longitudinal Rod-Beam model $2m = 6$	$\begin{Bmatrix} u \\ w \\ \theta_y \\ N_x \\ V_z \\ M_y \end{Bmatrix}$	$\begin{Bmatrix} 0 \\ 0 \\ 0 \\ -q_x \\ -q_z \\ -m_y \end{Bmatrix}$	$\begin{bmatrix} 0 & 0 & 0 & 1/EA & 0 & 0 \\ 0 & 0 & 0 & 0 & 1/GA_z & 0 \\ 0 & 0 & 0 & 0 & 0 & 1/EI_y \\ -\rho A\omega^2 & 0 & 0 & 0 & 0 & 0 \\ 0 & -\rho A\omega^2 & 0 & 0 & 0 & 0 \\ 0 & 0 & -\rho I_y \omega^2 & 0 & 0 & 0 \end{bmatrix}$

Table 1: The generalized beam without scatterers. Definition of state-vector $\mathbf{u}(x)$, force vector $\mathbf{q}(x)$ and matrix of parameters \mathbf{A} for several different types of elastic waveguides, those with: purely longitudinal waves, purely torsional waves, purely flexural waves and coupled problems.

A particularly illustrative demonstration of this approach can be observed in the comparison between the Euler-Bernoulli and Timoshenko beam models (refer to entries 5 and 6 in Table 1). Typically, the Timoshenko model is depicted in literature as a system of second-order partial differential equations concerning displacement and rotation, contrasting with the Euler-Bernoulli model, which is traditionally viewed as a classical fourth-order equation focusing on displacement exclusively. However, in this context, we'll adopt a unified approach for both models, augmenting the matrix \mathbf{A} with additional terms to incorporate considerations for shear deformation and rotational inertia.

In the development of our approach, it becomes of special interest the dispersion relation of the host generalized beam, i.e. without scatterers, which somehow represents the unperturbed dispersion relation. Considering Eq. (2) in absence of external loads $\mathbf{q}(x) \equiv \mathbf{0}$, we can check for solutions of the form $\mathbf{u}(x) = \hat{\mathbf{u}} e^{ikx}$ leading to the following eigenvalue problem

$$[\mathbf{A} - ik \mathbf{I}] \hat{\mathbf{u}} = \mathbf{0} \quad (3)$$

where \mathbf{I} stands for the identity matrix of size $2m$ and k represents the wavenumber. Any waveguide governed by the matrix \mathbf{A} with state-vector $\mathbf{u}(x)$ will present in general $2m$ modes, with m modes corresponding to rightwards waves and m modes corresponding to leftwards waves. These modes can be either propagating or evanescent depending on the complex nature of wavenumber k . For instance, longitudinal waves in rods have $m = 1$ propagating modes in each direction. Low frequency flexural waves present $2m = 4$ modes, one propagating and one evanescent for both rightward and leftward waves. High frequency beam waves (Timoshenko beam) present $m = 2$ propagating modes at each direction (bending and shear waves). Denoting \mathbf{u}_j and \mathbf{v}_j to be the right and left eigenvectors associated to each mode with eigenvalue ik_j , i.e. for the matrix \mathbf{A} governing the conserved quantities along the empty-waveguide

$$\mathbf{A} \mathbf{u}_j = ik_j \mathbf{u}_j, \quad \mathbf{v}_j^T \mathbf{A} = ik_j \mathbf{v}_j^T, \quad \mathbf{v}_j^T \mathbf{u}_l = \delta_{jl}, \quad 1 \leq j, l \leq 2m \quad (4)$$

where δ_{jl} denotes the Kronecker delta function.

We define a unit cell of length L along the waveguide and place N scatterers inside at different and arbitrary local positions ξ_1, \dots, ξ_N (see fig 1). The global positions of the scatterers respect to certain fixed reference point can be expressed as

$$x_{p\alpha} = pL + \xi_\alpha, \quad p = 0, \pm 1, \pm 2, \dots, \quad 1 \leq \alpha \leq N \quad (5)$$

We will differentiate between two types of scatterers:

Resonators: Either discrete or continuous elastic attached substructures can be considered, depending on whether they have a finite or infinite number of internal resonance frequencies, respectively. The resonator vibrates according to the internal resonances inducing forces back through the attachment point, radiating the effect to the rest of the host medium. Mathematically, each resonator is characterized by a frequency-dependent transfer matrix $\mathbf{T}^{(\alpha)}$ locally-defined along its length, which relates generalized degrees of freedom and forces between the attaching point and the free end.

Inclusions: We define inclusions as those regions, defined along the waveguide and of relatively small size with respect to the wavelength, where the material and/or section properties change. These perturbations of the beam properties induce changes in the transmission pattern and generate reflections. We consider that each inclusion is homogeneous along its width Δx_α and inside the waves are traveling according to Eq. (2) but with another different properties, say \mathbf{A}_α , different to \mathbf{A} , generating a perturbation.

In both cases, the perturbations induce certain radiating forces located at the scatterers, giving rise to the scattered field. Thus, the total wavefield can be obtained introducing certain external concentrated forces as located at the scatterers with the form

$$\mathbf{q}(x) = \sum_p \sum_{\alpha=1}^N \mathbf{K}_\alpha \mathbf{u}(x_{p\alpha}) \delta(x - x_{p\alpha}) \quad (6)$$

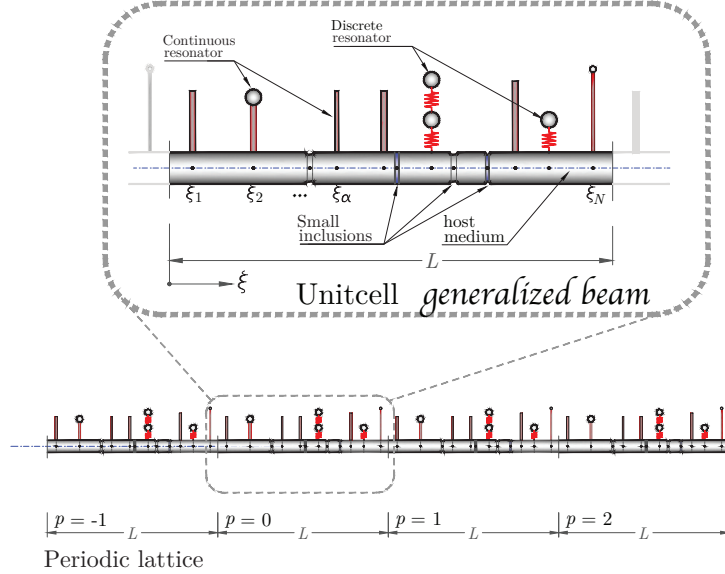


Figure 1: Generalized beam: phononic crystal formed by a 1D waveguide with an arbitrary number N of scatterers distributed in the unit cell of length L . The 1D structure has properties arranged in matrix \mathbf{A} , see Table 1. The scatterers considered can be of two types: (1) linear resonators attached pointwise to the waveguide and (2) small-width inclusions with other material or changes in cross-sectional dimensions. The properties of scatterers are introduced in matrices \mathbf{K}_α , see Table 2

where $\delta(x)$ stands for the Dirac-delta function and $\mathbf{u}(x_{p\alpha})$ is the state-vector evaluated at the α th scatterer at the p th unit cell. The $2m \times 2m$ -matrix \mathbf{K}_α is characteristic of each scatterer and depends on whether it is a resonator-type or a inclusion-type, showing a completely different form in both cases. The \mathbf{K}_α matrix has been derived for resonator-type and inclusion-type scatterers in references [51, 52], respectively. In Appendix A and Appendix B, some details on the derivations can be found, useful from a practice point of view. Table 2 summarizes these results.

The combination of the host-medium, whose properties are contained within matrix \mathbf{A} , and the N arbitrarily distributed scatterers characterized by the set of N matrices \mathbf{K}_α , constitute together the new proposed concept called *generalized beam*. Unifying Eqs. (2) and (6), the generalized beam obeys the following differential equation

$$\frac{d\mathbf{u}}{dx} = \mathbf{A} \mathbf{u} + \sum_p \sum_{\alpha=1}^N \mathbf{K}_\alpha \mathbf{u}(x_{p\alpha}) \delta(x - x_{p\alpha}) \quad (7)$$

We devote the following sections to derive its dispersion relationship as function of these general input parameters, enabling the application of the method to a vast variety of phononic structures governed Eq. (7).

3. Dispersion relationship

3.1. Exact solution

In this section, we will derive exact equations which define the dispersion relation of any 1D waveguide governed by the differential equation (7) in the frequency domain. Our objective is to find the nature of

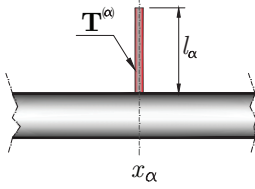
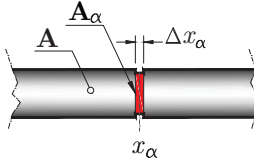
Type of scatterer	Resonators	Inclusions
Standing wave equation	$\frac{d\mathbf{u}}{dx} = \mathbf{A}\mathbf{u} + \sum_p \sum_{\alpha=1}^N \mathbf{K}_\alpha \mathbf{u}(x_\alpha) \delta(x - x_{p\alpha})$	
Matrix \mathbf{K}_α	$\left[\begin{array}{c c} \mathbf{0} & \mathbf{0} \\ \hline \mathbf{H} \mathbf{T}_{ff}^{(\alpha)-1} \mathbf{T}_{fd}^{(\alpha)} & \mathbf{H}^T \end{array} \right]$	$e^{-\mathbf{A} \Delta x_\alpha / 2} \quad e^{\mathbf{A}_\alpha \Delta x_\alpha / 2} \quad - \quad e^{\mathbf{A} \Delta x_\alpha / 2} \quad e^{-\mathbf{A}_\alpha \Delta x_\alpha / 2}$
Sketch		

Table 2: Both resonators and small inclusions in 1D beam-like structures have the same mathematical consideration in the dispersion relations, but under a different form of \mathbf{K}_α matrix. For resonators-type scatterers: matrix \mathbf{K}_α depends on the block-matrices of the transfer matrix $\mathbf{T}^{(\alpha)}$ associated to the whole scatterer and on the matrix \mathbf{H} which allows to relate degrees of freedom of the end of the scatterer with those of the beam-axis (detailed info in Appendix A and in ref. [52]). For inclusions-type scatterers: matrix \mathbf{K}_α depends uniquely on both matrices \mathbf{A} and \mathbf{A}_α associated to the properties of the host-medium and scatterer-medium (detailed info in Appendix B and in ref. [51]).

propagating waves, characterized by a wavenumber k and a waveform $\mathbf{u}(x)$, which in general are related each other when invoking the Bloch theorem, namely

$$\mathbf{u}(x) = e^{ikx} \Psi(x) \quad (8)$$

where k is the wavenumber and $\Psi(x)$ is an unknown periodic function with periodicity L to be found for each value of k (wavemode). By periodic conditions we can expand in Fourier coefficients yielding

$$\Psi(x) = \sum_{\nu=-\infty}^{\infty} \mathbf{W}_\nu e^{iq_\nu x} \quad , \quad q_\nu = \frac{2\pi\nu}{L} \quad , \quad pL \leq x \leq (p+1)L \quad (9)$$

where now the sequence of coefficients $\{\mathbf{W}_\nu\}_{\nu=-\infty}^{\infty}$ are unknown $2m$ -size arrays to be found. Plugging Eq. (9) into Eq. (B.10) we obtain after some arrangements

$$\sum_{\nu=-\infty}^{\infty} [i(k + q_\nu)\mathbf{I} - \mathbf{A}] \mathbf{W}_\nu e^{iq_\nu x} = \sum_p \sum_{\alpha} \mathbf{K}_\alpha \Psi(x_{p\alpha}) e^{-ik(x-x_{p\alpha})} \delta(x - x_{p\alpha}) \quad (10)$$

Premultiplying by $e^{-iq_\mu x}$ and integrating in any unit cell, i.e. $\int_{x=pL}^{(p+1)L} (\bullet) e^{-iq_\mu x} dx$, it yields

$$\sum_{\nu=-\infty}^{\infty} [(k + iq_\nu)\mathbf{I} - \mathbf{A}] \mathbf{W}_\nu \delta_{\mu\nu} L = \sum_{\alpha=1}^N \mathbf{K}_\alpha \Psi(\xi_\alpha) e^{-iq_\mu \xi_\alpha} \quad (11)$$

where $\delta_{\mu\nu}$ stands for the Kronecker delta-function, leading to

$$[i(k + q_\mu)\mathbf{I} - \mathbf{A}] \mathbf{W}_\mu L = \sum_{\alpha=1}^N \mathbf{K}_\alpha \Psi(\xi_\alpha) e^{-iq_\mu \xi_\alpha} \quad (12)$$

Expressing the vectors $\Psi(\xi_\alpha)$ also in terms of the Fourier coefficients as $\Psi(\xi_\alpha) = \sum_{\nu=-\infty}^{\infty} \mathbf{W}_\nu e^{iq_\nu \xi_\alpha}$ we obtain

$$[i(k + q_\mu)\mathbf{I} - \mathbf{A}] \mathbf{W}_\mu L = \sum_{\nu=-\infty}^{\infty} \sum_{\alpha=1}^N \mathbf{K}_\alpha \mathbf{W}_\nu e^{i(q_\nu - q_\mu) \xi_\alpha} \quad (13)$$

The above relations represents an eigenvalue problem with eigenvalue k and where the eigenvector is represented by the infinite set $\{\mathbf{W}_\mu\}_{\mu=-\infty}^{\infty}$. Since for each index μ , \mathbf{W}_μ is a $2m$ -sized vector, we can work in the spectral basis of matrix \mathbf{A} given by Eqs. (4), expanding in terms of the right-eigenvectors $\{\mathbf{u}_l\}_{l=1}^{2m}$, resulting in $2m$ coefficients $a_l(\mu)$

$$\mathbf{W}_\mu = \sum_{l=1}^{2m} a_l(\mu) \mathbf{u}_l \quad (14)$$

or in a more compact form just

$$\mathbf{W}_\mu = \mathbf{U} \mathbf{a}(\mu) \quad (15)$$

where $\mathbf{U} = [\mathbf{u}_1, \dots, \mathbf{u}_{2m}]$ is the square matrix of size $2m$ with the elements of basis $\{\mathbf{u}_l\}_{l=1}^{2m}$ as columns, and $\mathbf{a}(\mu) = \{a_1(\mu), \dots, a_{2m}(\mu)\}^T$ stands for the $2m$ coefficients of \mathbf{W}_μ in such basis. Plugging this expression into Eq. (13)

$$[i(k + q_\mu)\mathbf{I} - \mathbf{A}] \mathbf{U} \mathbf{a}(\mu) L = \sum_{\nu=-\infty}^{\infty} \sum_{\alpha=1}^N \mathbf{K}_\alpha \mathbf{U} \mathbf{a}(\nu) e^{i(q_\nu - q_\mu) \xi_\alpha} \quad (16)$$

Similarly as above we can build the matrix $\mathbf{V} = [\mathbf{v}_1, \dots, \mathbf{v}_{2m}]$ with the left-eigenvectors of \mathbf{A} . Premultiplying by \mathbf{V}^T and using the orthogonal relationships of Eq. (4) in matrix form $\mathbf{V}^T \mathbf{A} \mathbf{U} = i\mathbf{k}_0 = \text{diag}[ik_1, \dots, ik_{2m}]$ and $\mathbf{V}^T \mathbf{U} = \mathbf{I}_{2m}$, we find an equivalent expression to that of Eq. (13) but now with the additional advantage that the left-hand side of the equation is diagonal

$$iL[(k + q_\mu)\mathbf{I}_{2m} - \mathbf{k}_0] \mathbf{a}(\mu) = \sum_{\nu=-\infty}^{\infty} \sum_{\alpha=1}^N \mathbf{V}^T \mathbf{K}_\alpha \mathbf{U} \mathbf{a}(\nu) e^{i(q_\nu - q_\mu) \xi_\alpha} \quad (17)$$

Using a more compact form for the right-hand side, it yields

$$iL[(k + q_\mu)\mathbf{I}_{2m} - \mathbf{k}_0] \mathbf{a}(\mu) = \sum_{\nu=-\infty}^{\infty} \mathbf{H}(\mu, \nu) \mathbf{a}(\nu) \quad , \quad \mu = 0, \pm 1, \pm 2, \dots \quad (18)$$

where the matrices $\mathbf{H}(\mu, \nu)$ are defined as

$$\mathbf{H}(\mu, \nu) = \sum_{\alpha=1}^N \mathbf{V}^T \mathbf{K}_\alpha \mathbf{U} e^{i(q_\nu - q_\mu) \xi_\alpha} \quad (19)$$

Truncating the series by using $2M + 1$ plane waves, i.e. $-M \leq \nu, \mu \leq M$, the previous system of equations takes now the form of the finite linear eigenvalue problem in the parameter $\lambda = ikL$

$$\left(\hat{\mathbf{H}} + \mathbf{D} \right) \hat{\mathbf{a}} = \lambda \hat{\mathbf{a}} \quad (20)$$

Above \mathbf{D} is a diagonal matrix of size $2m \times (2M + 1)$ with the following structure

$$\mathbf{D} = \begin{bmatrix} iL(\mathbf{k}_0 - q_{-M}\mathbf{I}_{2m}) & \cdots & \mathbf{0}_{2m} \\ \vdots & \ddots & \vdots \\ \mathbf{0}_{2m} & \cdots & iL(\mathbf{k}_0 - q_M\mathbf{I}_{2m}) \end{bmatrix} \quad (21)$$

On the other side, the matrix $\hat{\mathbf{H}}$ and eigenvector $\hat{\mathbf{a}}$ are also blocks-made matrices

$$\hat{\mathbf{H}} = \begin{bmatrix} \mathbf{H}(-M, -M) & \mathbf{H}(-M, -M+1) & \cdots & \mathbf{H}(-M, M) \\ \mathbf{H}(-M+1, -M) & \mathbf{H}(-M+1, -M+1) & \cdots & \mathbf{H}(-M+1, M) \\ \vdots & \vdots & \ddots & \vdots \\ \mathbf{H}(M, -M) & \mathbf{H}(M, -M+1) & \cdots & \mathbf{H}(M, M) \end{bmatrix}, \quad \hat{\mathbf{a}} = \begin{Bmatrix} \mathbf{a}(-M) \\ \mathbf{a}(-M+1) \\ \vdots \\ \mathbf{a}(M) \end{Bmatrix} \quad (22)$$

Making use of the Kronecker product and some abuse in the notation we can express the above matrices in a way meaningfully shorter. If we introduce the column vector $\mathbf{q} = \{q_{-M}, \dots, q_M\}^T$, we can define the following vector and matrix

$$e^{i\mathbf{q}\xi_\alpha} = \begin{Bmatrix} e^{iq_{-M}\xi_\alpha} \\ \vdots \\ e^{iq_M\xi_\alpha} \end{Bmatrix}, \quad e^{i\mathbf{q}^T\xi_\alpha} = \{e^{iq_{-M}\xi_\alpha}, \dots, e^{iq_M\xi_\alpha}\}, \quad \mathbf{Q} = \text{diag}[q_{-M}, \dots, q_M] = \begin{bmatrix} q_{-M} & \cdots & 0 \\ \vdots & \ddots & \vdots \\ 0 & \cdots & q_M \end{bmatrix} \quad (23)$$

Resulting in the expressions

$$\begin{aligned} \hat{\mathbf{H}} &= \sum_{\alpha=1}^N \left(e^{-i\mathbf{q}\xi_\alpha} \cdot e^{i\mathbf{q}^T\xi_\alpha} \right) \otimes (\mathbf{V}^T \mathbf{K}_\alpha \mathbf{U}) \\ \mathbf{D} &= \mathbf{I}_{2M+1} \otimes \mathbf{k}_0 - \mathbf{Q} \otimes \mathbf{I}_{2m} \end{aligned} \quad (24)$$

This notation can be specially useful for the numerical implementation. The procedure described here is accurate for solving the dispersion relation of the model presented in Eq. (7). Recall that the model of Eq. (7) reproduces exactly the behavior of media with point-connected resonators, but introduces errors when attempting to reproduce the behavior of a medium with inclusions. Therefore, it is expected that the solution of the eigenvalue problem (20) will be affected by errors inherited from the approximation of inclusions as point-sources, as described in ref. [51]. Numerical examples validate this procedure in the context of 1D phononic crystals. Next, some semi-analytical procedures will be presented to find approximations of the dispersion relation for weakly scattered media.

3.2. Approximate solutions based on weak scattering

The introduction of disturbances in the medium modifies the behavior of the waves. It is well known that at some frequencies band gaps emerge, which prevent the wave from propagating. However, the reality is that in the presence of weak scattering, wave propagation is verified at the vast majority of frequencies, albeit in a slightly different way than in a homogeneous medium. In this section, we are particularly interested in shedding light on how the wave is perturbed in the presence of N scatterers as those shown in Table 2 along a span of length L and obtaining the dispersion relation. We do not expect the approximate solutions to reproduce accurately the dispersion relation within band gaps, as we shall see in the numerical examples.

Looking at general eigenvalue problem of Eq. (17), and canceling the effect of scatterers then the problem reduces to

$$iL [\mathbf{k}_0 - q_\nu \mathbf{I}_{2m}] \mathbf{a}_0(\nu) = \lambda \mathbf{a}_0(\nu) \quad , \quad -\infty < \nu < \infty \quad (25)$$

where $\{\mathbf{a}_0(\nu)\}_{\nu=-\infty}^{\infty}$ stands for the wavemode coefficients of the homogenous host-beam free of scatterers. This a trivial diagonal eigenvalue problem in the parameter λ , where the solutions depends on two indexes (j, ν), so each eigenvalue can be expressed as one element of the infinite set

$$\lambda(j, \nu) = \{ik_j L - iq_\nu L : 1 \leq j \leq 2m, -\infty \leq \nu \leq \infty\} \quad (26)$$

And the corresponding eigenvector $\{\mathbf{a}_0(\mu) \in \mathbb{C}^{2m} : -\infty < \mu < \infty\}$ associated to the eigenvalue $ik_jL - iq_\nu L$ is

$$\mathbf{a}_0(\mu) = \begin{cases} \mathbf{0} \in \mathbb{C}^{2m} & \text{if } \mu \neq \nu \\ \{0, \dots, 0, \underbrace{1}_{\text{pos. } j}, 0, \dots, 0\}^T & \text{if } \mu = \nu \end{cases} \quad (27)$$

Taking into account these coefficients and following Eqs. (9) and (14), the eigenmode can then readily be written simply as

$$\Psi_0(\xi) = e^{iq_\nu \xi} \mathbf{u}_j \quad (28)$$

Fixed the index j , every mode of the form $\lambda = \pm ik_jL - iq_\nu L$ for $\nu = 0, \pm 1, \pm 2, \dots$ represents an additional branch in the irreducible Brillouin zone corresponding to the bare generalized beam. In order to visualize the meaning of these eigenvalues the different branches $k_jL - q_\nu L$, with $-3 \leq \nu \leq 3$ have been plotted in Fig. 2 for a steel Euler-Bernoulli beam with a cross section of dimensions 50x100 mm. As known, the left/right bending propagating modes have respectively the expressions $k_{1,3} = \pm (\rho A \omega^2 / EI)^{1/4}$ (the other two modes k_2 and k_4 are evanescent, see Appendix C). Notice that the different branches within the Brillouin zone are equivalent to folding up that one corresponding to $q_0 = 0$.

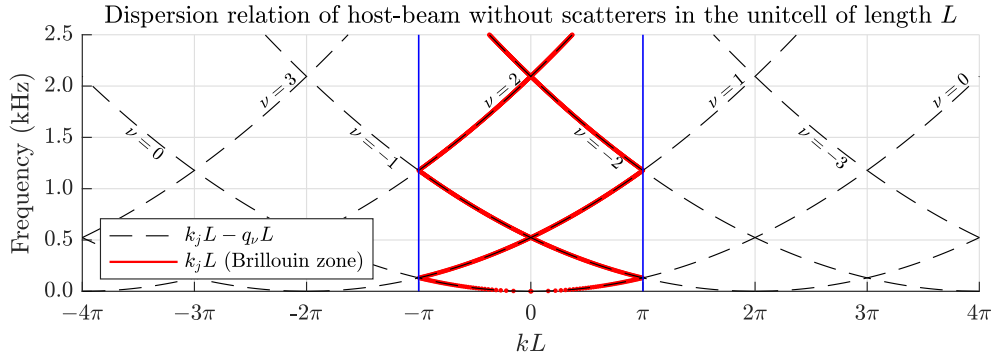


Figure 2: Dispersion relationship of the bare host-beam without scatterers. The different branches are corresponding to expressions of the form $k_jL - q_\nu$, $q_\nu = 2\pi\nu/L$, $\nu = 0, \pm 1, \pm 2, \dots$. Within the Brillouin zone, they constitute the same curve as folding the branch $q_0 = 0$.

For the oncoming developments we will refer to each one of these modes with the duple (j, ν) . Let us fix one mode of the unperturbed beam, say (j, ν) , and assume that the arrangement of scatterers produce just a slight perturbation of the dispersion relation. Each one of the modes of Eq. (26) will be perturbed and the components of the eigenvector $\{a_l(\mu) : 1 \leq l \leq 2m, -\infty < \mu < \infty\}$ will vary slightly respect to those shown in Eq. (27). Since we can choose any type of normalization, we will impose that

$$a_j(\nu) = 1 \quad , \quad \text{normalization relationship for mode } (j, \nu) \quad (29)$$

The eigenvalue $\lambda = ikL$ and the eigenvector $\mathbf{a}(\mu)$, $-\infty < \mu < \infty$ are related by means of Eq. (17) which we rewrite that corresponding the generic plane wave ν .

$$iL [(k + q_\nu)\mathbf{I}_{2m} - \mathbf{k}_0] \mathbf{a}(\nu) = \sum_{\mu=-\infty}^{\infty} \sum_{\alpha=1}^N \mathbf{V}^T \mathbf{K}_\alpha \mathbf{U} \mathbf{a}(\mu) e^{i(q_\mu - q_\nu) \xi_\alpha} \quad (30)$$

This eigenvalue problem presented above cannot be solved analytically, and the plane wave series must be truncated as described in the previous section, for practical applications. However, some analytical expressions can be derived by taking advantage of the remarkable decoupling of the left-hand side terms in Eq. (30). Ultimately, these expressions will enable us to design an iterative procedure that can, under certain conditions, find the exact solution. Furthermore, the first and second iterations easily lead to expressions

that can serve as a suitable analytical solution for problems with weak scattering.

Assume that we know the form of the eigenmode given by the periodic function $\Psi(x)$. If we focus on the j th relationship of Eq. (30) we have

$$iL[(k + q_\nu - k_j)a_j(\nu)] = \sum_{\alpha=1}^N \mathbf{v}_j^T \mathbf{K}_\alpha \Psi(\xi_\alpha) e^{-iq_\nu \xi_\alpha} \quad (31)$$

where the definition of the function $\Psi(\xi) = \sum_{\mu} \sum_l a_l(\mu) \mathbf{u}_l e^{iq_\mu \xi}$ has been used from Eqs. (9) and (14). Using now the normalization relationship $a_j(\nu) = 1$ of Eq. (29), we can readily have the value of k as function of the eigenmode $\Psi(\xi)$

$$k = k_j - q_\nu + \frac{1}{iL} \sum_{\alpha=1}^N \mathbf{v}_j^T \mathbf{K}_\alpha \Psi(\xi_\alpha) e^{-iq_\nu \xi_\alpha} \quad (32)$$

On the other side, consider now that the eigenvalue k is known but so not the coefficients of eigenmode, $\mathbf{a}(\nu)$. From Eq. (31) changing the index j by the generic l and solving for $a_l(\nu)$, we find

$$a_l(\nu) = \sum_{\alpha=1}^N \mathbf{v}_l^T \mathbf{K}_\alpha \Psi(\xi_\alpha) \frac{e^{-iq_\nu \xi_\alpha}}{iL[k - k_l + q_\nu]} \quad (33)$$

The mode is then

$$\Psi(\xi) = \sum_{\nu=-\infty}^{\infty} \sum_{l=1}^{2m} a_l(\nu) \mathbf{u}_l e^{iq_\nu \xi} = \sum_{\nu=-\infty}^{\infty} \sum_{l=1}^{2m} \mathbf{u}_l \left(\sum_{\alpha=1}^N \mathbf{v}_l^T \mathbf{K}_\alpha \Psi(\xi_\alpha) \frac{e^{-iq_\nu \xi_\alpha}}{iL[k - k_l + q_\nu]} \right) e^{iq_\nu \xi} \quad (34)$$

After some rearrangements, this expression can be written much more compact as

$$\Psi(\xi) = \sum_{\alpha=1}^N \mathbf{G}(k, \xi - \xi_\alpha) \mathbf{K}_\alpha \Psi(\xi_\alpha) \quad (35)$$

where the function $\mathbf{G}(k, \xi) \in \mathbb{C}^{2m \times 2m}$ is a matrix for each pair (k, ξ) and is defined as

$$\mathbf{G}(k, \xi) = \sum_{l=1}^{2m} \mathbf{u}_l \mathbf{v}_l^T \varphi(k - k_l, \xi) \quad (36)$$

Above, the new function $\varphi(\kappa, \xi)$ captures the waveform periodicity and has the simple expression

$$\varphi(\kappa, \xi) = \sum_{\nu=-\infty}^{\infty} \frac{e^{iq_\nu \xi}}{iL(\kappa + q_\nu)} \quad (37)$$

which can even be more simplified since its sum can be obtained as the periodic expansion by Fourier series to the whole axis x of the following closed-form expression, defined in the interval $[0, L]$

$$\varphi(\kappa, \xi) = \frac{e^{-i\kappa \xi}}{1 - e^{-i\kappa L}}, \quad 0 \leq \xi \leq L \quad (38)$$

The notation of the function $\mathbf{G}(k, x)$ has not been chosen arbitrarily since it is close related to the Green function of the homogeneous medium under certain configuration of applied forces. Indeed, consider that at the locations $x_p = pL$, , $p = 0, \pm 1, \pm 2, \dots$ a source of magnitude e^{ikx_p} is applied. The Green function in such situation is the k -dependent matrix $\mathbf{U}(k, x)$ which verifies the following differential equation

$$\left(\frac{d}{dx} - \mathbf{A} \right) \mathbf{U} = \sum_{p=-\infty}^{\infty} \mathbf{I} e^{ikpL} \delta(x - pL) \quad (39)$$

x

Then, it can be proved that this Green function is indeed $\mathbf{U}(k, x) = e^{ikx} \mathbf{G}(k, x)$, where $\mathbf{G}(k, x)$ has been defined in Eq. (36). The matrix $\mathbf{G}(k, x)$ stands for the periodic response of the homogeneous medium to a periodic distribution of point sources every L meters.

Evaluating now Eq. (35) at $\xi = \xi_1, \dots, \xi_N$ we find the following system of $2mN$ algebraic equations

$$\begin{pmatrix} \Psi(\xi_1) \\ \Psi(\xi_2) \\ \vdots \\ \Psi(\xi_N) \end{pmatrix} = \begin{bmatrix} \mathbf{G}(k, 0)\mathbf{K}_1 & \mathbf{G}(k, \xi_1 - \xi_2)\mathbf{K}_2 & \cdots & \mathbf{G}(k, \xi_1 - \xi_N)\mathbf{K}_N \\ \mathbf{G}(k, \xi_2 - \xi_1)\mathbf{K}_1 & \mathbf{G}(k, 0)\mathbf{K}_2 & \cdots & \mathbf{G}(k, \xi_2 - \xi_N)\mathbf{K}_N \\ \vdots & \vdots & \ddots & \vdots \\ \mathbf{G}(k, \xi_N - \xi_1)\mathbf{K}_1 & \mathbf{G}(k, \xi_N - \xi_2)\mathbf{K}_2 & \cdots & \mathbf{G}(k, 0)\mathbf{K}_N \end{bmatrix} \begin{pmatrix} \Psi(\xi_1) \\ \Psi(\xi_2) \\ \vdots \\ \Psi(\xi_N) \end{pmatrix} \quad (40)$$

Introducing the new notation

$$\hat{\Psi} = \begin{pmatrix} \Psi(\xi_1) \\ \Psi(\xi_2) \\ \vdots \\ \Psi(\xi_N) \end{pmatrix}, \quad \hat{\mathbf{G}}(k) = \begin{bmatrix} \mathbf{G}(k, 0) & \mathbf{G}(k, \xi_1 - \xi_2) & \cdots & \mathbf{G}(k, \xi_1 - \xi_N) \\ \mathbf{G}(k, \xi_2 - \xi_1) & \mathbf{G}(k, 0) & \cdots & \mathbf{G}(k, \xi_2 - \xi_N) \\ \vdots & \vdots & \ddots & \vdots \\ \mathbf{G}(k, \xi_N - \xi_1) & \mathbf{G}(k, \xi_N - \xi_2) & \cdots & \mathbf{G}(k, 0) \end{bmatrix}, \quad \hat{\mathbf{K}} = \begin{bmatrix} \mathbf{K}_1 & \cdots & \mathbf{0}_{2m} \\ \vdots & \ddots & \vdots \\ \mathbf{0}_{2m} & \cdots & \mathbf{K}_N \end{bmatrix} \quad (41)$$

we find that the vector $\hat{\Psi}$ is obtained as function of the eigenvalue k , solving the null subspace associated to the unitary eigenvalue of matrix $\hat{\mathbf{G}}(k)\hat{\mathbf{K}}$, i.e.

$$\left[\mathbf{I}_{2mN} - \hat{\mathbf{G}}(k)\hat{\mathbf{K}} \right] \hat{\Psi} = \mathbf{0} \quad (42)$$

As shown above, we can express the wavenumber k as function of $\Psi(x)$ in Eq. (32) and inversely the wavemode $\Psi(x)$ as function of k from Eq. (35) just solving the null-space problem (42). And more important is the fact that these expressions are exact and expressed in terms of the eigenmode evaluated at the scatterers. In what follows we will exploit these new relationships to generate an iterative scheme. Fixed a mode of the unperturbed beam, say (j, ν) , consider the following initial values, corresponding to the bare waveguide

$$k^{(0)} = k_j - q_\nu, \quad \Psi_0(\xi) = e^{iq_\nu \xi} \mathbf{u}_j \quad (43)$$

The values of $k^{(0)}$ have been plotted in Fig. 2 for an Euler–Bernoulli beam, showing the different branches which arise after evaluating $q_\nu = 2\pi\nu/L$, for $\nu = 0, \pm 1, \pm 2, \dots$. We define the following sequences $\{k^{(n)}\}$ and $\{\Psi_n(\xi)\}$ for $n = 1, 2, \dots$

$$k^{(n)} = k_j - q_\nu + \frac{1}{iL} \sum_{\alpha=1}^N \mathbf{v}_j^T \mathbf{K}_\alpha \Psi_{n-1}(\xi_\alpha) e^{-iq_\nu \xi_\alpha} \quad (44)$$

$$\Psi_n(\xi) = \sum_{\alpha=1}^N \mathbf{G}(k^{(n)}, \xi - \xi_\alpha) \mathbf{K}_\alpha \Psi_{n-1}(\xi_\alpha) \quad (45)$$

According to the presented scheme, each mode (j, ν) , with $1 \leq j \leq 2m$ and $-M \leq \nu \leq M$ can be obtain by perturbation, following the recursive method presented above. However, as shown in Fig. 2, the modes for $\nu = \pm 1, \pm 2, \dots$ are just branches that can be obtained folding that of $\nu = 0$ in the irreducible Brillouin zone. Therefore we can just keep working with the mode $(j, 0)$ or shortly the j th mode. Moreover, since only the evaluation of the wavemodes at the scatterers, say $\Psi_{n-1}(\xi_\alpha)$, is needed we can rewrite the above sequences in a more compact form using the structure of the extended vector $\hat{\Psi}$ and matrices $\hat{\mathbf{G}}(k)$ and $\hat{\mathbf{K}}$ defined in Eq. (41), resulting

$$k^{(n)} = k_j + \frac{1}{iL} (\mathbf{1}_N^T \otimes \mathbf{v}_j^T) \hat{\mathbf{K}} \hat{\Psi}_{n-1} \quad (46)$$

$$\hat{\Psi}_n = \hat{\mathbf{G}}(k^{(n)}) \hat{\mathbf{K}} \hat{\Psi}_{n-1} \quad (47)$$

where we use the notation $\mathbf{1}_N^T \otimes \mathbf{v}_j^T$ to represent the row-vector formed by \mathbf{v}_j^T , replicated N times. The vector $\mathbf{1}_N = \{1, \dots, 1\}^T$ of size N denotes the column vector of size N formed only by ones.

First and second order iterations have a qualitative value since analytical expressions can be derived. Indeed the first order perturbation of the mode $(j, 0)$ leads to

$$k^{(1)} = k_j + \frac{1}{iL} \sum_{\alpha=1}^N \mathbf{v}_j^T \mathbf{K}_\alpha \mathbf{u}_j \quad (48)$$

The second iteration is now proportional to the first-order mode, yielding

$$k^{(2)} = k_j + \frac{1}{iL} \sum_{\alpha=1}^N \mathbf{v}_j^T \mathbf{K}_\alpha \Psi_1(\xi_\alpha) \quad (49)$$

where the vectors $\Psi_1(\xi_\alpha)$ can be evaluated from the expression of the first iteration

$$\begin{aligned} \Psi_1(\xi_\alpha) &= \sum_{\beta=1}^N \mathbf{G}(k^{(1)}, \xi_\alpha - \xi_\beta) \mathbf{K}_\beta \Psi_0(\xi_\beta) \\ &= \sum_{\alpha=1}^N \sum_{l=1}^{2m} \mathbf{u}_l \mathbf{v}_l^T \varphi(k^{(1)} - k_l, \xi_\alpha - \xi_\beta) \mathbf{K}_\alpha \mathbf{u}_j \end{aligned} \quad (50)$$

Plugging this expression into Eq. (49) and considering the particular case with all scatterers equal, say $\mathbf{K}_\alpha = \mathbf{K}_0$, $1 \leq \alpha \leq N$, then, after some rearrangements we have

$$k^{(2)} = k_j + \frac{1}{iL} \sum_{l=1}^{2m} (\mathbf{v}_j^T \mathbf{K}_0 \mathbf{u}_l) (\mathbf{v}_l^T \mathbf{K}_0 \mathbf{u}_j) \zeta(k^{(1)} - k_l) \quad (51)$$

where the function $\zeta(k)$ is defined as

$$\zeta(k) = \sum_{\alpha} \sum_{\beta} \varphi(k, \xi_\alpha - \xi_\beta) \quad (52)$$

Using the periodic expansion of $\varphi(k, \xi)$ given in Eq. (37) this function can be expressed in series as

$$\zeta(k) = \sum_{\nu=-\infty}^{\infty} \frac{NS(q_\nu)}{iL(k + q_\nu)} \quad (53)$$

where $S(q)$ stands for the structure factor of the distribution of points

$$S(q) = \frac{1}{N} \sum_{\alpha=1}^N \sum_{\beta=1}^N e^{-iq(\xi_\alpha - \xi_\beta)} \quad (54)$$

The expression of the 2nd order solution, i.e. Eq. (51), provides significantly more information than Eq. (48). It considers the impedance of the scatterers and their impact on the dispersion of mode j by accounting for all modes present in the beam through the coupling coefficients $\mathbf{v}_j^T \mathbf{K}_0 \mathbf{u}_l$ and $\mathbf{v}_l^T \mathbf{K}_0 \mathbf{u}_j$. Additionally, the weight factor given by the function $\zeta(k)$ links the geometrical distribution of points in the reciprocal space, via the Structure Factor, to the scattering properties of the medium. The $\zeta(k)$ function is singular at the coordinates of the reciprocal space, allowing us to interpret the factor $\zeta(k^{(1)} - k_l)$ as an interference coefficient in the mode j when an incident wavenumber k_l propagates through the medium. If the difference between the scattered wavenumber $k^{(1)}$ and the incident wavenumber k_l corresponds to a crystal lattice node in the reciprocal space, the interference is maximized. This represents the von Laue formulation and the Oswald sphere in 1D waveguides.

4. Convergence of the iterative scheme

Before validating the expressions obtained in the previous section, it is worth asking under what conditions the convergence of the iterative scheme occurs. This is relevant in order to predict the behavior over a range of frequencies. Recalling the form of the sequences, it is straightforward that the sequence of wavenumbers $\{k^{(n)}\}$ will converge provided that the sequence of wavemodes does. In order to derive some mathematical condition for the convergence of this procedure, it turns out that in the Eq. (47), the recursive sequence of eigenmodes can be reduced to a fixed-point iterative scheme. Indeed, consider the following function $\phi : \mathbb{C}^{2mN} \rightarrow \mathbb{C}$ associated to the unperturbed mode $(j, 0)$

$$\phi(\mathbf{X}) = k_j + \frac{1}{iL} (\mathbf{1}_N^T \otimes \mathbf{v}_j^T) \hat{\mathbf{K}} \mathbf{X} \quad , \quad \mathbf{X} \in \mathbb{C}^{2mN} \quad (55)$$

It is then clear that for each iteration we obtain $k^{(n)} = \phi(\hat{\Psi}_{n-1})$. Let us define the vector selfmapping $\mathbf{F}(\mathbf{X}) : \mathbb{C}^{2mN} \rightarrow \mathbb{C}^{2mN}$ as

$$\mathbf{F}(\mathbf{X}) = \hat{\mathbf{G}}[\phi(\mathbf{X})] \hat{\mathbf{K}} \mathbf{X} \quad (56)$$

Under these conditions the sequence of eigenmodes $\{\hat{\Psi}_n\}_{n \geq 1}$ can be generated just evaluating

$$\hat{\Psi}_n = \mathbf{F}(\hat{\Psi}_{n-1}) \quad , \quad \hat{\Psi}_0 = \mathbf{1}_N \otimes \mathbf{u}_j \quad (57)$$

This scheme is locally convergent if the spectral radius of the Jacobian is less than the unity when evaluated at the fixed-point, in this case at $\mathbf{X} = \hat{\Psi}$, which can be symbolized by

$$\rho\left(\frac{\partial \mathbf{F}}{\partial \mathbf{X}}\right) < 1 \quad , \quad \text{at } \mathbf{X} = \hat{\Psi} \quad (58)$$

where $\rho(\cdot)$ denotes the spectral radius of a matrix. The expression of the Jacobian is available analytically just using the chain rule in the differentiation and being consistent with the dimensions of the resulting expression to obtain a valid matrix.

$$\mathbf{J} = \frac{\partial \mathbf{F}}{\partial \mathbf{X}} = \frac{1}{iL} \left[\frac{\partial \hat{\mathbf{G}}[\phi(\mathbf{X})]}{\partial k} \cdot \hat{\mathbf{K}} \right] \mathbf{X} (\mathbf{1}_N^T \otimes \mathbf{v}_j^T) \hat{\mathbf{K}} + \hat{\mathbf{G}}[\phi(\mathbf{X})] \hat{\mathbf{K}} \quad (59)$$

This matrix turns out to be a good indicator of the validity of weak scattering based approaches. In the numerical examples, its value can be visualized for the frequency ranges studied. In general, the scheme converges quite quickly at the points where Eq. (58) holds. Even at points where it diverges locally, the first two iterations presented in the previous section usually give satisfactory results.

5. Example 1: Beam with point-resonators

In the first example an Euler-Bernoulli beam with $N = 5$ attached resonators along a $L = 1$ m long unit cell is studied. The dynamical properties of the beam are a mass per unit of length of $\rho A = 21$ kg/m, a sectional stiffness of $EI_y = 583$ m²kN. Each resonator has a mass of $m_\alpha = 0.3$ kg and a resonance of $\omega_\alpha = 5.4$ kHz. It is known that among the four wavemodes obtained from the dispersion relation of the bare beam, two are propagating and two evanescent. The matrix \mathbf{A} has now size 4×4 and its corresponding eigenvalues and eivectors, say $\lambda_j = ik_j$, \mathbf{u}_j and \mathbf{v}_j are sorted so that the two first represents the two traveling rightwards and the two last modes are evanescent, resulting

$$k_1 = -\kappa_f \quad , \quad k_2 = -i\kappa_f \quad , \quad k_3 = +\kappa_f \quad , \quad k_4 = +\kappa_f \quad , \quad (60)$$

where $\kappa_f = (\omega^2 \rho A / EI)^{1/4}$. Eigenvectors are listed in Appendix C. each resonator exerts a single vertical force on the beam proportional to the vertical displacement. We find only one nonzero element in the matrix

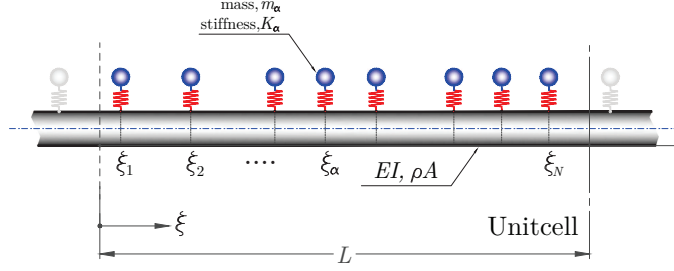


Figure 3: An Euler-Bernoulli beam with point single dof resonators.

\mathbf{K}_α , resulting the expression

$$\mathbf{K}_\alpha = m_\alpha \frac{\omega_\alpha^2 \omega^2}{\omega^2 - \omega_\alpha^2} \begin{bmatrix} 0 & 0 & 0 & 0 \\ 0 & 0 & 0 & 0 \\ 1 & 0 & 0 & 0 \\ 0 & 0 & 0 & 0 \end{bmatrix} \quad (61)$$

As seen in the theoretical derivations, the scatterers' information (position and dynamic properties) and the modes of the bare beam are sufficient to estimate in closed form the new dispersion relation as a perturbation of the four modes shown in Eq. (60). In what follows we will obtain the closed forms resulting from the first and second order perturbations of mode 1, i.e. $k_1 = -\kappa_f$. For the rest of modes, analog expressions can be found. Thus, the first order iteration can be found explicitly from Eq. (48), yielding for this particular case

$$k^{(1)} = -\kappa_f \left(1 - \sum_\alpha \frac{m_\alpha}{4\rho AL} \frac{\omega_\alpha^2}{\omega^2 - \omega_\alpha^2} \right) \quad (62)$$

which in the case of all scatterers equal with $m_\alpha = m_r$ and $\omega_\alpha = \omega_r$, yields

$$k^{(1)} = -\kappa_f \left(1 - \frac{Nm_r}{4\rho AL} \frac{\omega_r^2}{\omega^2 - \omega_r^2} \right) \quad (63)$$

The results of this expression are shown in Fig. 4, where both the dispersion relation of the evanescent mode in Fig. 4(a) and the propagating mode in Fig. 4(b) have been plotted. The latter is obtained by folding Eq. (63) into the irreducible Brillouin zone. The derived expression is continuous for all frequencies except at the scatterer resonances. It accounts for the number of scatterers, N , but not their distribution. Generally, the expression captures the change in wave velocity in regions away from the resonances, respect to the behaviour without resonators. It can also be seen how the model is also able to predict the dispersion of the evanescent mode and how it is affected by the resonance, resulting in a fairly accurate prediction.

Figure 4(c) illustrates the spectral radius of the Jacobian matrix, $\rho(\mathbf{J})$, as derived in Eq. (59). This spectral radius is crucial for assessing the convergence of the iterative method. When $\rho(\mathbf{J})$ is less than 1, the method converges locally to the exact mode, indicating that it is attractive. However, if $\rho(\mathbf{J})$ exceeds 1, the exact mode becomes a repulsive fixed point, preventing the method from reaching the accurate value. This parameter reflects the influence of both Bragg peaks and model resonances, as well as bandgaps. In regions where $\rho(\mathbf{J})$ is greater than 1, the results begin to diverge after a few iterations.

The effect of the scatterer distribution and the interaction of the perturbed mode with the other modes is captured by the second-order approximation derived in Eqs. (49) and (51). Applying this expression to the current example, where all scatterers are identical and the influence of evanescent modes is neglected in

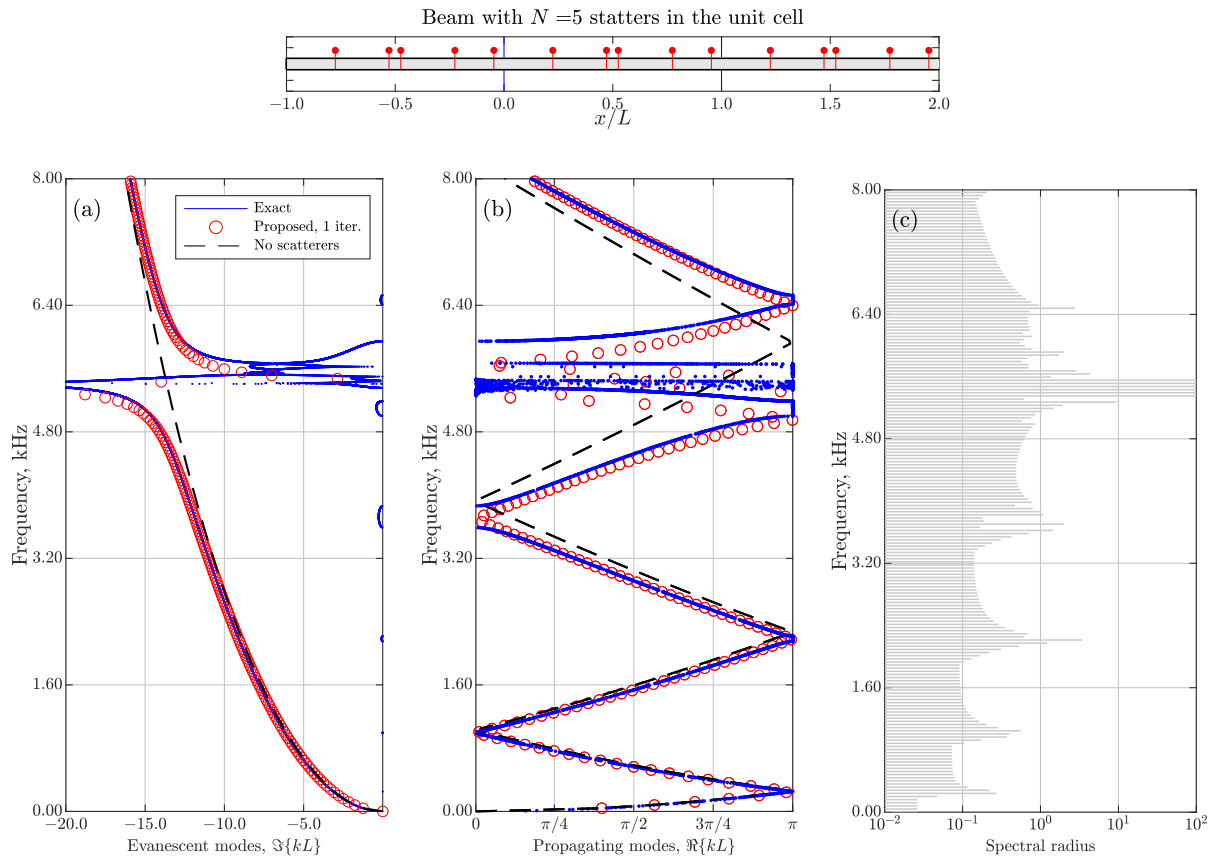


Figure 4: (a) and (b) Imaginary and real part of dispersion relation in Example 1, respectively. Exact result (blue), Iterative approach with the first-order iteration (red markers) and unperturbed homogeneous solution (dashed-black). (c) Plot of the spectral radius of the Jacobian matrix \mathbf{J} , criterium of convergence is $\rho(\mathbf{J}) < 1$

the sum of the modes, we obtain after some rearrangements the following expression

$$k^{(2)} = -\kappa_f + \frac{1}{L} \left(\frac{\kappa_f m_r}{4\rho A} \frac{\omega_r^2}{\omega^2 - \omega_r^2} \right)^2 \left[\zeta \left(k^{(1)} + \kappa_f \right) - \zeta \left(k^{(1)} - \kappa_f \right) \right] \quad (64)$$

Here, $\zeta(k)$ represents the function introduced in Eq. (53), which relates the distribution of points to the wavenumber of the medium through the structure factor. This function is singular at the coordinates of the medium's reciprocal space. In the specific case of Eq.(64), this property implies that at frequencies where the difference between the scattered wavenumber and that of the homogeneous medium matches a node of the reciprocal crystal lattice, scattering and interference reach their maximum (von Laue formulation). This effect is shown in Fig. 5(b), where the effect of these singularities emerges close to the frequencies associated to the Bragg peaks of the medium. It is observed that the second-order approximation provides a better fit to the exact dispersion relation in regions where the spectral radius $\rho(\mathbf{J}) < 1$.

6. Example 2: Rods and beams with inclusions

In this section, the proposed method will be applied in waveguides with small inclusions. We consider inclusions as perturbations in the cross-sectional properties and/or the waveguide material, which take place in a small segment dx , see Fig. 1. Perturbed properties can affect the propagating modes in the medium.

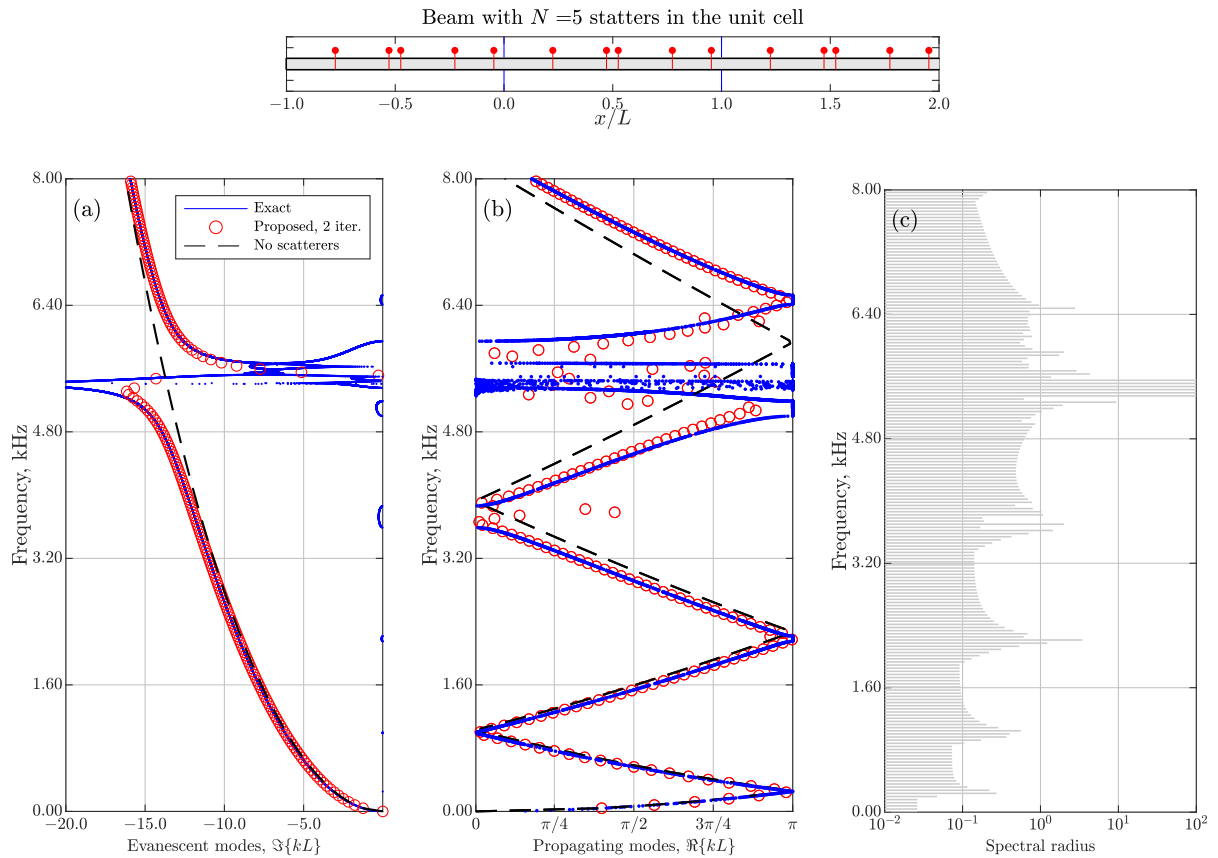


Figure 5: (a) and (b) Imaginary and real part of dispersion relation in Example 1, respectively. Exact result (blue), Iterative approach with the second-order iteration (red markers) and unperturbed homogeneous solution (dashed-black). (c) Plot of the spectral radius of the Jacobian matrix \mathbf{J} , criterium of convergence is $\rho(\mathbf{J}) < 1$

We will study two cases here: classical longitudinal waves in a rod and high-order flexural waves of a Timoshenko beam (bending and shear waves).

Let's consider first an aluminum bar with a cross-section of 5×5 cm, in which inclusions of another material with a different cross-section are periodically placed every 20 cm. The mechanical properties of the inclusions relative to the properties of the homogeneous medium are:

$$\rho A_\alpha = 0.45 \rho A, \quad EA_\alpha = 0.45 EA, \quad \Delta x_\alpha = 0.1h \quad (65)$$

where $EA = 1.75 \times 10^5$ kN and $\rho A = 5.3$ kg/m and $h = 5$ cm are the mechanical/geometrical properties of the bare aluminum rod. In Fig 6, the dispersion relation of the heterogeneous medium is shown. The chosen frequency range lies between 25 kHz and 32 kHz, including the region around the bandgap corresponding to the Bragg frequency $\omega_B = \frac{2\pi N}{L} \sqrt{E/\rho} \approx 29$ kHz.

The proposed model predicts that frequency bands with strong scattering are associated with greater values of the spectral radius of the Jacobian matrix \mathbf{J} defined in Eq. (59). In Fig 6(a) some particular frequencies have been studied, points P1 to P5. In Figs. 6(c) and 6(d) the relative iteration errors both for wavenumber and wavemodes sequences associated to these frequencies have been plotted. The relative

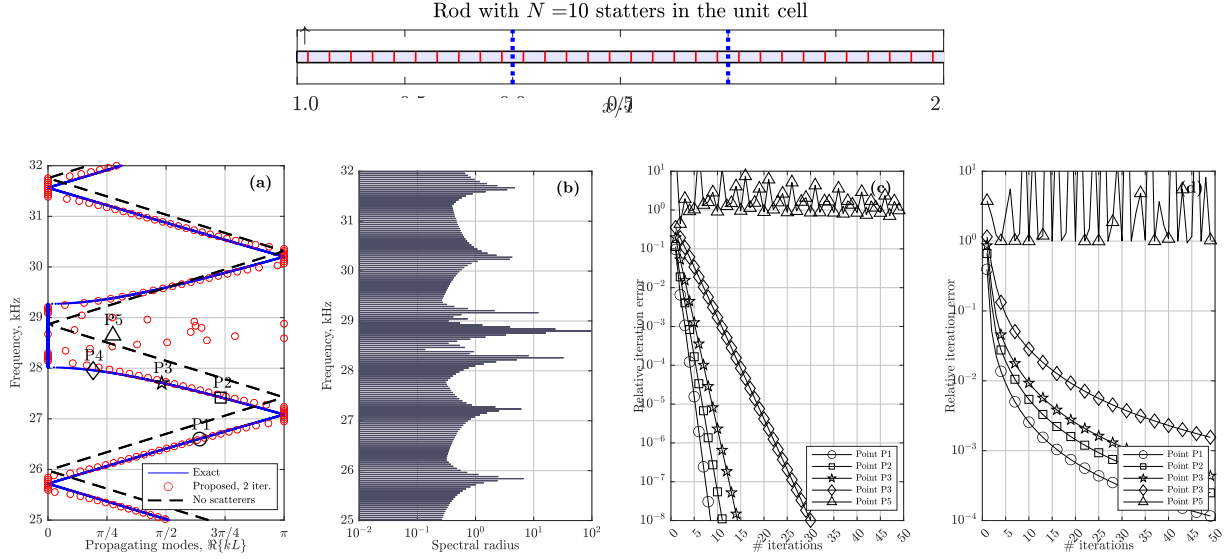


Figure 6: (a) Dispersion relation of Example 2 (real part) using two iterations. Exact result (blue), Iterative approach with the second-order iteration (red markers) and unperturbed homogeneous solution (dashed-black). (b) Plot of the spectral radius of the Jacobian matrix \mathbf{J} , criterion of convergence is $\rho(\mathbf{J}) < 1$, (c) and (d) Plot of iteration-error for wavenumbers and wavevectors respectively for each one of the the four frequencies P1 to P4 shown in (a)

iteration error both for wavenumbers and wavemodes are defined respectively

$$\text{Iteration error (wavenumber)} = \frac{|k^{(n+1)} - k^{(n)}|}{|k^{(n+1)}|}, \quad \text{Iteration error (mode)} = \frac{\|\Psi_{n+1} - \Psi_n\|}{\|\Psi_{n+1}\|} \quad (66)$$

It is observed that the sequence of wavenumbers and modes does not converge in this case for the frequency at point P5, which corresponds to a spectral radius larger than one. However, the above sequences do converge at other frequencies where the spectral radius is less than one, as observed for points P1, P2, P3 and P4. In these cases, the convergence speed is inversely proportional to the value of the spectral radius at that frequency. The scattering diagram shown in Fig. 6(a) corresponds to the 2nd order solution which, as can be seen, is sufficiently accurate for practical purposes.

It should be noted that the scheme converges but not towards the exact solution, since the model based on multiple scattering of Eq. (B.10), based on the use of equation (B.9) for the matrix \mathbf{K}_α , carries an approximation error that depends on the contrast of properties between scatterers and medium [51]. Despite the error accumulation, the proposed model reproduces quite well the dispersion relation in regions outside the bandgaps.

The proposed approach is also suitable for modeling the dispersion relationship of flexural waves in beams with perturbations in the cross-section and material, regardless of the beam model used. Figure 7 shows the results obtained for a 12×12 cm cross-section Timoshenko beam that reproduces both flexural and shear waves. The properties of the bare beam without perturbations are

$$EI = 1210 \text{ kNm}^2, \quad GA = 2.45 \times 10^5 \text{ kNm}, \quad \rho A = 30.2 \text{ kg/m}, \quad \rho I = 0.036 \text{ kg m}^2/\text{m}, \quad \omega_c = 13 \text{ kHz} \quad (67)$$

where ω_c represents the cutoff frequency, which separates the frequency range into two regions. For frequencies $\omega < \omega_c$, the medium exhibits a propagating mode associated with flexural waves, which, for very low frequencies, say $\omega < 0.05\omega_c$, coincides with the dispersion of the Euler-Bernoulli beam. Conversely, for $\omega > \omega_c$, in addition to the flexural mode, the shear deformation mode appears. Using the host medium

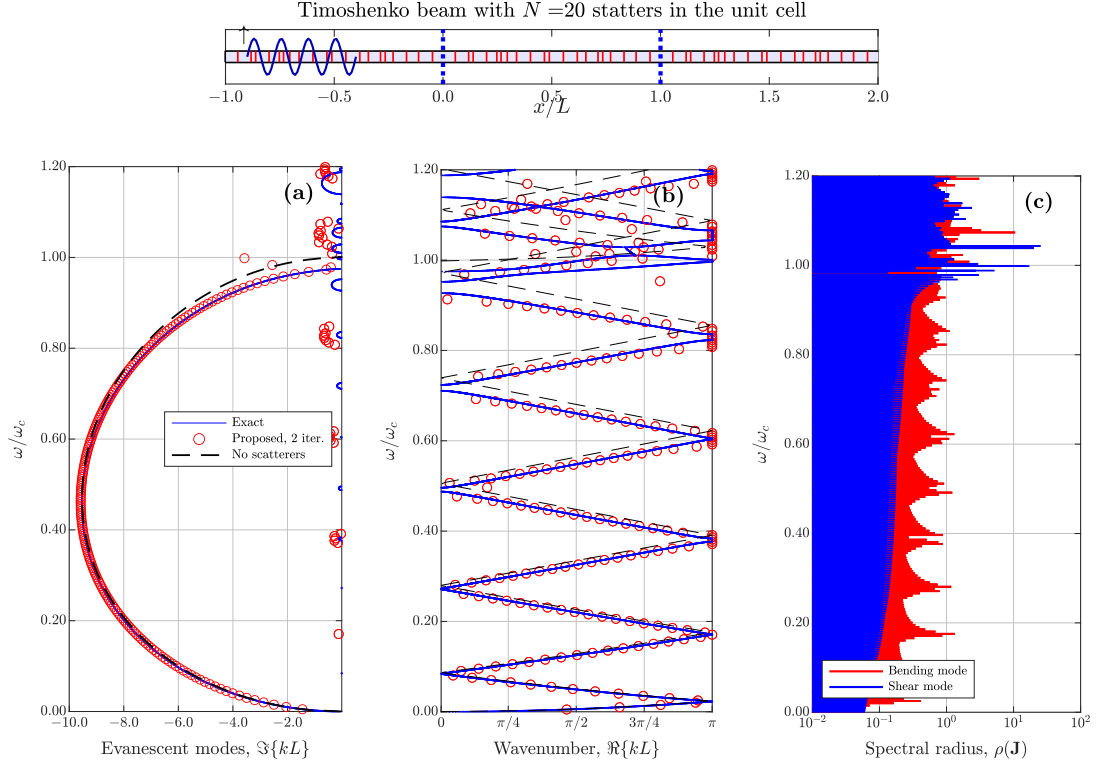


Figure 7: (a) and (b) Imaginary and real part respectively of dispersion relation in Example 2, using the second-order iteration (Timoshenko beam with small inclusions of other material). Exact result (blue), Iterative approach with the second-order iteration (red markers) and unperturbed homogeneous solution (dashed-black). (c) Plot of the spectral radius of the Jacobian matrix \mathbf{J} , criterion of convergence is $\rho(\mathbf{J}) < 1$. In red, spectral radius associated to bending mode. In blue, spectral radius associated to shear mode

described above, we introduce a total of $N = 20$ small inclusions of another material, randomly distributed within a unit cell of length $L = 1$ m. The mechanical properties of the cross-section in the inclusions are

$$EI_\alpha = 1.4 EI, \quad GA_\alpha = 1.4 GA, \quad \rho A_\alpha = 1.5 \rho A, \quad \rho I_\alpha = 1.50 \rho I, \quad \Delta x_\alpha = 0.15h \quad (68)$$

Figures 7(a) and 7(b) show the imaginary and real parts of the wavenumber, respectively, while Figure 7(c) reproduces the spectral radius $\rho(\mathbf{J})$ associated with the convergence of the algorithm, which in this case can be evaluated for the two modes present in the waveguide. Below the cutoff frequency, the dispersion occurs due to the interaction between scatterers. The bandgaps are not particularly wide because there is no correlation between the inclusions. This leads to a good approximation of the proposed model in the range $0 < \omega < \omega_c$, both for the dispersion of propagating waves and evanescent waves. In the latter case, it can be observed in Figure 7(a) that the model predicts the value of the evanescent wavenumber when it existed in the medium without scatterers, such as the case of the evanescent flexural modes. However, the imaginary value in the bandgaps that arise from the introduction of inclusions is not reproduced coherently with the proposed procedure, as they are not strictly a perturbation of any mode.

The spectral radius can be evaluated for all existing modes and is represented in Figure 7(c), with the shear mode (evanescent at low frequencies) in blue and the flexural mode in red. At low frequencies, the interaction of the flexural waves with the scatterers due to their periodic positioning is observed. However, there is hardly any interaction between the evanescent waves due to their own nature, resulting in a low spectral radius and consequently a good estimation of the wavenumber with one or two iterations. The

modes present in the beam below the cutoff frequency do not interact with each other in the absence of scatterers in the beam. However, the introduction of these scatterers induces coupling between the flexural and shear branches for frequencies $\omega > \omega_c$. This effect, along with the interaction of each mode with the scatterers, increases the spectral radius of the matrix \mathbf{J} and thereby the scattering in the medium, causing the iterative procedure to diverge.

7. Example 3: Waveguide with attached beams

In the last example, some results will be presented for the case of a waveguide in which $N = 10$ beam-resonators, capable of vibrating transversely and longitudinally, have been embedded. The host beam is aluminum with a square cross-section of dimensions $h \times b = 12 \times 12$ cm, with the same properties as those presented in the previous example, reproduced in Eq. (67). The resonators are also made of aluminum and have a cross-section of $h_\alpha \times b_\alpha = 2.4 \times 2.4$ cm and a length of $l_\alpha = 24$ cm. The natural frequencies of the longitudinal and flexural vibration modes of the resonators are listed in Table 3.

	ω_1/ω_c	ω_2/ω_c	ω_3/ω_c
Longitudinal modes	0.460	1.380	2.300
Flexural modes	0.030	0.186	0.521

Table 3: Natural frequencies of the beam-resonators relative to the cutoff frequency of the host-beam

Figure 8 shows the dispersion diagram for the beam with the resonators. The two possible propagation modes can be distinguished: longitudinal modes (horizontal displacement, $u(x)$) and flexural modes (vertical displacement, $w(x)$). On the other hand, the resonators can vibrate longitudinally or transversely. In the first case, vertical forces are induced, which modify the flexural modes of the medium. In the second case, horizontal forces and moments are induced in the beam, modifying both the longitudinal and flexural modes in the medium. Thus, breaks in the flexural bands of the beam can be seen at frequencies $\omega/\omega_c = 0.03, 0.186, 0.46, 0.52$. In the regions around the resonances, bandgaps open with significant scattering. At other frequencies, the wave behavior reflects significant changes compared to the modes of the bare beam (represented by a black dashed line). Despite this, the proposed model reproduces the dispersion pattern quite accurately, as shown in Figure 8, using 2 iterations, see Eq. (51). Again, several propagation modes through the medium allow the spectral radius of the Jacobian matrix \mathbf{J} to be evaluated for each of them, resulting in Figure 8(c), where the regions reflect the measure of the perturbation of each mode and allow diagnosing the quality of the iterative procedure.

We will conclude the presentation of the results of this last example by showing the propagation modes for some specific frequencies. The results are shown in Figure 9. It is worth noting that in this case, each mode includes both horizontal displacement $u(x)$ and vertical displacement $w(x)$. In the left column, Figures 9(a), 9(c), 9(e) show the horizontal displacement, while in the right column, Figures 9(b), 9(d), 9(f) show the vertical displacement. The modes obtained after 2 iterations, 10 iterations, and infinite iterations (exact mode case) are reproduced. Note that the three cases represented correspond to convergent simulations, as reflected by the spectral radius of each mode considered. The first two rows reproduce the longitudinal and flexural modes dispersed in the medium for the frequency $\omega = 0.90\omega_c$. The longitudinal mode exhibits polarization in the transverse direction due to the presence of the resonators. The displacement $w(x)$ shown in Figure 9(b) is smooth, as the rotations of the cross-sections are continuous functions. However, the horizontal displacement $u(x)$ that arises in the flexural mode, Figure 9(c), has abrupt changes in the derivative. This is quite accurately reflected by the model and reproduces the horizontal forces induced by the resonators. Note that the changes in slope coincide with the positions of the resonators, represented by black dots. The perturbation of a shear mode for the frequency $\omega = 1.93\omega_c$ is shown in the last row, Figures 9(e) and 9(f). This frequency is very high relative to the Timoshenko model, and the use of this model to evaluate the behavior at such a frequency could be debated. However, the model works perfectly

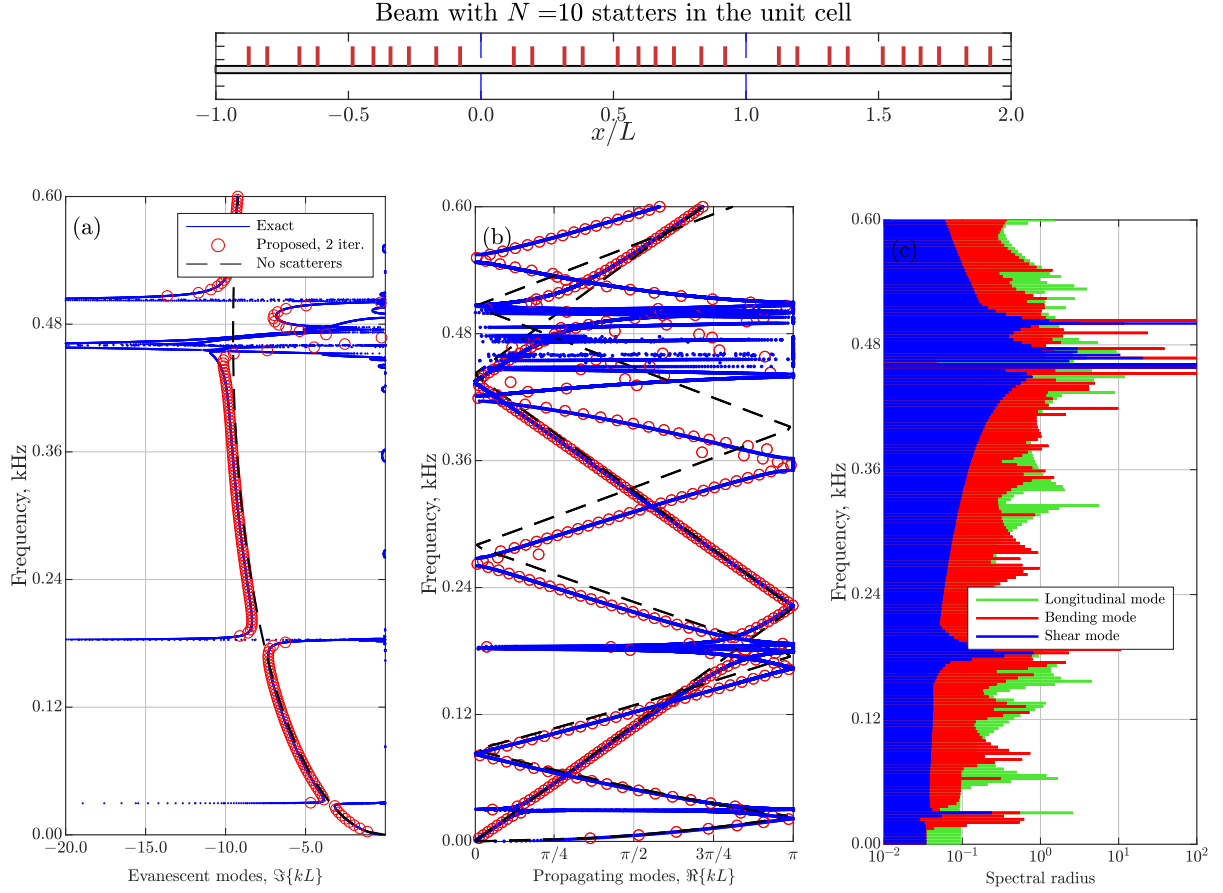


Figure 8: (a) and (b) Imaginary and real part respectively of dispersion relation in Example 3, using the second-order iteration (Timoshenko beam with continuous resonators). Exact result (blue), Iterative approach with the second-order iteration (red markers) and unperturbed homogeneous solution (dashed-black). (c) Plot of the spectral radius of the Jacobian matrix \mathbf{J} , criterion of convergence is $\rho(\mathbf{J}) < 1$. In green, spectral radius associated to the longitudinal mode of the beam. In red, bending mode and in blue, the shear mode

and once again shows that the accuracy does not depend on the frequency but on the scattering in the wave dispersion, reflected by the mean spectral radius $\rho(\mathbf{J})$, whose value in this case does not exceed unity, ensuring the convergence and feasibility of using the proposed approach.

8. Conclusions

In this article, we address the solution of the dispersion relation in periodic structures formed by a one-dimensional elastic support, where an arbitrary number of scatterers are located in the unit cell. The problem is treated in a general manner, as the derived mathematical model is applicable to any elastic waveguide, assuming that the radiation forces generated by scatterers are proportional to the field. We refer to the resulting model as the generalized beam. The dispersion relation is obtained using the plane wave expansion method. Under the assumption of weak scattering, an iterative procedure is developed, where the initial iterations provide approximate analytical expressions that explicitly predict wave propagation, offering valuable qualitative insights. Additionally, strict convergence conditions for the method are deduced and validated through several numerical examples, covering various types of waveguides and scatterers.

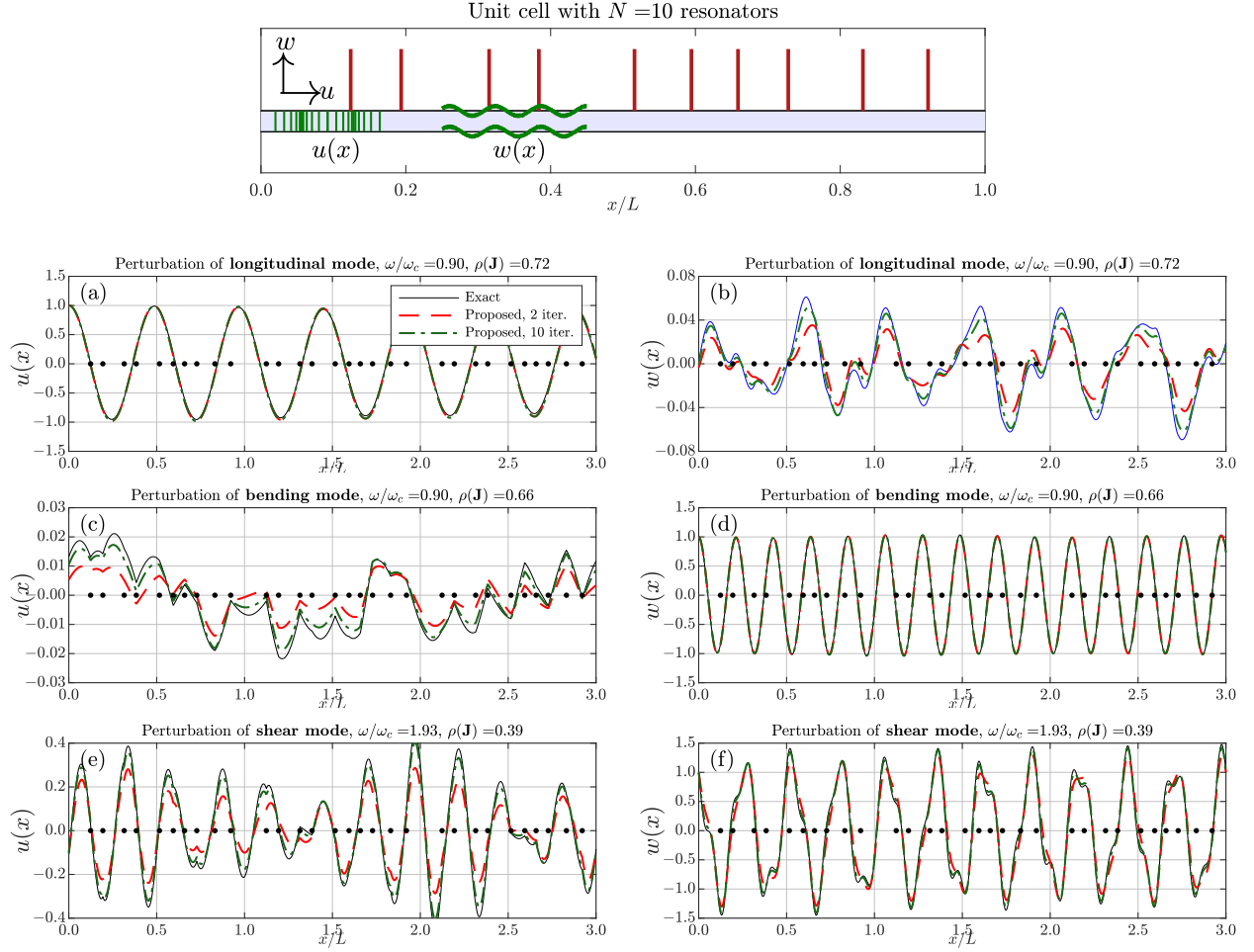


Figure 9: Representation of propagating longitudinal, bending and shear modes for Example 3 obtained for a frequency of $\omega/\omega_c = 0.90$. Left plots, (a), (c) and (e) represent the horizontal displacement $u(x)$. Right plots, (b), (d) and (e) depicts the vertical displacement. In black, the exact mode, in red the proposed approximate method with two iterations, in blue with 10 iterations.

Appendix A. Matrix \mathbf{K}_α for resonators-type scatterers

In case of resonator-type scatterers, they are attached to the host medium at certain point of its boundary, say R (see fig. A.10). If we define certain local axes (η, ζ) with R as origin, we can define a vector with degrees of freedom and generalized forces along the resonator, say $\mathbf{d}^{(\alpha)}(\eta)$, $\mathbf{f}^{(\alpha)}(\eta)$. The relationships between degrees of freedom and generalized forces between the two ends of the resonator is given by the transfer matrix $\mathbf{T}^{(\alpha)}$. Thus, we can write

$$\begin{Bmatrix} \mathbf{d}^{(\alpha)}(l_\alpha) \\ \mathbf{f}^{(\alpha)}(l_\alpha) \end{Bmatrix} = \mathbf{T}^{(\alpha)} \begin{Bmatrix} \mathbf{d}^{(\alpha)}(0) \\ \mathbf{f}^{(\alpha)}(0) \end{Bmatrix} = \begin{bmatrix} \mathbf{T}_{dd}^{(\alpha)} & \mathbf{T}_{df}^{(\alpha)} \\ \mathbf{T}_{fd}^{(\alpha)} & \mathbf{T}_{ff}^{(\alpha)} \end{bmatrix} \begin{Bmatrix} \mathbf{d}^{(\alpha)}(0) \\ \mathbf{f}^{(\alpha)}(0) \end{Bmatrix} \quad (\text{A.1})$$

In the current derivations, the transfer matrix $\mathbf{T}^{(\alpha)}$ is a $2m \times 2m$ array which depends on the resonator mechanical properties and on frequency, including possible added elastic or mass devices along the length l_α , resulting in such case the product of the different transfer matrices associated to each segment [53]. Splitting up the matrix $\mathbf{T}^{(\alpha)}$ in four $m \times m$ block-matrices, we can relate both displacements and internal

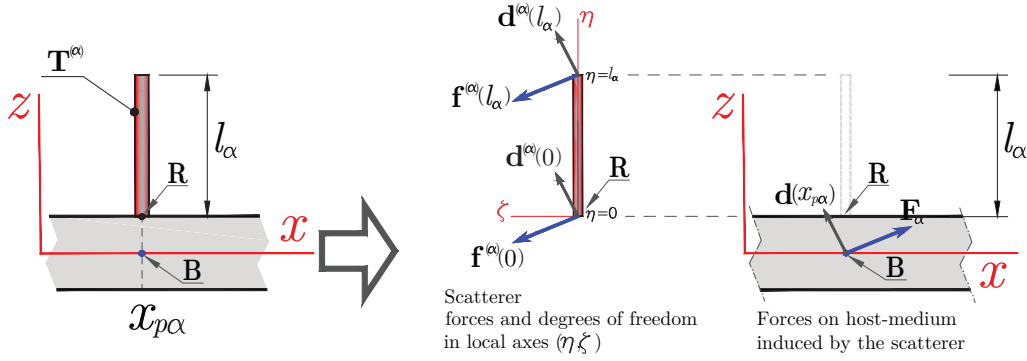


Figure A.10: The kinematic variables $\mathbf{d}^{(\alpha)}(\eta)$ and the generalized forces $\mathbf{f}^{(\alpha)}(\eta)$, in local axes of the resonator, are related to each other with the resonator's own transfer matrix, evaluated between the points $\eta = 0$ and $\eta = l_\alpha$, see Eq. (A.1). The effect on the waveguide-axis, point B, is given by the array with forces \mathbf{F}_α which is just the statically equivalent to forces $\mathbf{f}^{(\alpha)}$, located at the connection point between the waveguide and resonator, i.e. point R.

forces at both ends, $\eta = \{0, l_\alpha\}$, resulting in The opposite edge of the resonator at $\eta = l_\alpha$ is forces-free, therefore $\mathbf{f}^{(\alpha)}(l_\alpha) = \mathbf{0}$ leading to the equation

$$\mathbf{0} = \mathbf{T}_{fd}^{(\alpha)} \mathbf{d}^{(\alpha)}(0) + \mathbf{T}_{ff}^{(\alpha)} \mathbf{f}^{(\alpha)}(0) \quad (\text{A.2})$$

yielding

$$\mathbf{f}^{(\alpha)}(0) = - \left[\mathbf{T}_{ff}^{(\alpha)} \right]^{-1} \mathbf{T}_{fd}^{(\alpha)} \mathbf{d}^{(\alpha)}(0) \quad (\text{A.3})$$

However, the forces represented in the vector $\mathbf{f}^{(\alpha)}(0)$ are in the local axes of the resonator and are also located at point R. Forces \mathbf{F}_α in global axes (x, z) due to the effect of the resonator and acting on the waveguide axis (point B) are derived from equilibrium considerations, resulting in

$$\mathbf{F}_\alpha = \mathbf{H} \mathbf{f}^{(\alpha)}(0) \quad (\text{A.4})$$

On the other side, local displacements and rotations contained in vector $\mathbf{d}^{(\alpha)}(0)$ can be related with the global degrees of freedom at point B, say $\mathbf{d}(x_{p\alpha})$ using the kinematics of the cross-section, leading to the following expression

$$\mathbf{d}^{(\alpha)}(0) = \mathbf{H}^T \mathbf{d}(x_{p\alpha}) \quad (\text{A.5})$$

From Eqs. (A.3), (A.4) and (A.5), we obtain the following relationship between beam forces \mathbf{F}_α and displacements $\mathbf{d}(x_\alpha)$ in global axes (x, z)

$$\mathbf{F}_\alpha = -\mathbf{H} \mathbf{T}_{ff}^{(\alpha)-1} \mathbf{T}_{fd}^{(\alpha)} \mathbf{H}^T \mathbf{d}(x_\alpha) \quad (\text{A.6})$$

The point-forces can then be introduced into the differential equation (2) using the Dirac-delta function, resulting

$$\mathbf{q}_\alpha(x) = - \left\{ \begin{array}{c} \mathbf{0} \\ \mathbf{F}_\alpha \end{array} \right\} \delta(x - x_\alpha) = \left[\begin{array}{cc|cc} \mathbf{0} & \mathbf{0} & \mathbf{0} & \mathbf{0} \\ \mathbf{H} \mathbf{T}_{ff}^{(\alpha)-1} & \mathbf{T}_{fd}^{(\alpha)} \mathbf{H}^T & \mathbf{0} & \mathbf{0} \end{array} \right] \left\{ \begin{array}{c} \mathbf{d}(x_\alpha) \\ \mathbf{f}(x_\alpha) \end{array} \right\} \delta(x - x_\alpha) \equiv \mathbf{K}_\alpha \mathbf{u}(x_\alpha) \delta(x - x_\alpha) \quad (\text{A.7})$$

where the matrix \mathbf{K}_α is defined as

$$\mathbf{K}_\alpha = \left[\begin{array}{cc|cc} \mathbf{0} & \mathbf{0} & \mathbf{0} & \mathbf{0} \\ \mathbf{H} \mathbf{T}_{ff}^{(\alpha)-1} & \mathbf{T}_{fd}^{(\alpha)} \mathbf{H}^T & \mathbf{0} & \mathbf{0} \end{array} \right] \quad (\text{A.8})$$

Within the matrix \mathbf{K}_α we can find all properties of the resonators, including the set of resonances which will correspond to the roots of the equation

$$\det \left[\mathbf{T}_{ff}^{(\alpha)}(\omega) \right] = 0 \quad \rightarrow \quad \text{Resonance frequencies: } \omega_1, \omega_2, \dots \quad (\text{A.9})$$

Appendix B. Matrix \mathbf{K}_α for inclusions-type scatterers

If the scatterers turn out to be perturbations of the cross-sectional properties and/or changes in the material properties, what actually occurs is a jump in the value of the matrix that determines the behaviour of the waveguide as a homogeneous material. In such a situation the differential equation governing the state-vector along the waveguide is

$$\frac{d\mathbf{u}}{dx} = \mathcal{A}(x) \mathbf{u} + \mathbf{q}(x), \quad (\text{B.1})$$

where the function $\mathcal{A}(x)$ can be defined as the piecewise continuous function

$$\mathcal{A}(x) = \begin{cases} \mathbf{A}_\alpha & \text{if } x \in [x_{p\alpha} - \Delta x_\alpha/2, x_\alpha + \Delta x_\alpha/2] \\ \mathbf{A} & \text{if } x \notin [x_{p\alpha} - \Delta x_\alpha/2, x_\alpha + \Delta x_\alpha/2] \end{cases} \quad \alpha = 1, 2, \dots, N, \quad , \quad p = 0, \pm 1, \pm 2, \dots \quad (\text{B.2})$$

This function can be expressed mathematically in one single line as

$$\mathcal{A}(x) = \mathbf{A} + \sum_p \sum_{\alpha=1}^N (\mathbf{A}_\alpha - \mathbf{A}) \Delta H_\alpha(x - x_{p\alpha}), \quad (\text{B.3})$$

where

$$\Delta H_\alpha(x) = H\left(x + \frac{\Delta x_\alpha}{2}\right) - H\left(x - \frac{\Delta x_\alpha}{2}\right) \quad (\text{B.4})$$

stands for the finite step function of width Δx_α and centered at the origin, expressed in terms of the classical Heaviside's unit function, $H(x)$, equal to 0 for $x < 0$ and 1 for $x > 0$. Substituting Eq. (B.3) into Eq. (B.1) yields and making $\mathbf{q}(x) \equiv \mathbf{0}$ in order to study the nature of the propagating waves, it yields

$$\frac{d\mathbf{u}}{dx} = \mathbf{A} \mathbf{u} + \sum_p \sum_{\alpha=1}^N (\mathbf{A}_\alpha - \mathbf{A}) \mathbf{u}(x) \Delta H_\alpha(x - x_{p\alpha}) \quad (\text{B.5})$$

Denoting and defining $\mathbf{f}_r(x, \mathbf{u})$ to be the response of the inclusions, i.e.

$$\mathbf{f}_r(x, \mathbf{u}) = \sum_p \sum_{\alpha} (\mathbf{A}_\alpha - \mathbf{A}) \mathbf{u}(x) \Delta H_\alpha(x - x_{p\alpha}), \quad (\text{B.6})$$

The Eq. (B.5) can then be written as

$$\frac{d\mathbf{u}}{dx} = \mathbf{A} \mathbf{u} + \mathbf{f}_r(x, \mathbf{u}) \quad (\text{B.7})$$

The term $\mathbf{f}_r(x, \mathbf{u})$ can be interpreted as a radiated wavefield in response to an incident wave interacting with the scatterers within the waveguide. In the ref. [51] is demonstrated that the radiated field is solely due to $\mathbf{f}_r(x, \mathbf{u})$ and this vector can asymptotically be expressed as a series of outgoing sources to account for the contribution of every scatterer and to satisfy the Sommerfeld radiation condition at infinity [54].

$$\mathbf{f}_r(x, \mathbf{u}) \approx \sum_p \sum_{\alpha=1}^N \mathbf{K}_\alpha \mathbf{u}(x_\alpha) \delta(x - x_{p\alpha}), \quad (\text{B.8})$$

here the matrix \mathbf{K}_α is expressed in the following terms

$$\mathbf{K}_\alpha = e^{-\mathbf{A} \Delta x_\alpha / 2} e^{\mathbf{A}_\alpha \Delta x_\alpha / 2} - e^{\mathbf{A} \Delta x_\alpha / 2} e^{-\mathbf{A}_\alpha \Delta x_\alpha / 2}. \quad (\text{B.9})$$

with $e^{\mathbf{A} \Delta x_\alpha / 2}$ and $e^{\mathbf{A}_\alpha \Delta x_\alpha / 2}$ denoting exponential matrices. As shown above in Eqs. (6) and (B.8), it is proved that both the introduction of resonators and the consideration of inclusions receive the same mathematical treatment. The wave modes which can travel in this way therefore verify the differential equation

$$\frac{d\mathbf{u}}{dx} = \mathbf{A} \mathbf{u} + \sum_p \sum_{\alpha=1}^N \mathbf{K}_\alpha \mathbf{u}(x_{p\alpha}) \delta(x - x_{p\alpha}) \quad (\text{B.10})$$

where the nature of matrix \mathbf{K}_α is different depending on the type of scatterer. In Table 2 the form of each \mathbf{K}_α is shown.

Appendix C. Wavemodes of some waveguides

The modes of the bare one-dimensional waveguides (without scatterers) used for the numerical examples have been obtained analytically for the cases of longitudinal waves, flexural waves (Euler-Bernoulli beam), and flexural waves (Timoshenko beam). The results are presented in Table C.4, where some of the parameters used are common and are expressed in terms of the mechanical properties of the cross-sectional area. In the case of Example 3, the longitudinal and transverse waves are not coupled in the homogeneous medium, so the eigenvector solution is the composition in the form of 6-component vectors between the solutions of longitudinal waves and Timoshenko flexural waves shown in Table C.4.

$$\begin{aligned} \kappa_f &= \left(\omega^2 \frac{\rho A}{EI_y} \right)^{1/4} & \kappa_c &= \omega \sqrt{\frac{\rho A}{EA}} & \kappa_s &= \omega \sqrt{\frac{\rho A}{GA_z}} \\ r &= \sqrt{\frac{I_y}{A}} & \alpha &= \sqrt{\frac{\rho I_y GA_z}{\rho A EI_y}} = r \frac{\kappa_f^2}{\kappa_s} & \Omega &= \frac{\omega}{\omega_c} \\ \omega_c &= \sqrt{\frac{GA_z}{\rho I_y}} & \eta &= \sqrt{1 + \frac{4\alpha^2}{(1 + \alpha^2)^2} \frac{1 - \Omega^2}{\Omega^2}} \end{aligned} \quad (\text{C.1})$$

Acknowledgments

M.L. and V.R.-G. are grateful for the partial support under Grant No. PID2020-112759GB-I00 funded by MCIN/AEI/10.13039/501100011033. V.R.-G. acknowledge support from Grant No. CIAICO/2022/052 of the ‘‘Programa para la promoci3n de la investigaci3n cient3fica, el desarrollo tecnol3gico y la innovaci3n en la Comunitat Valenciana’’ funded by Generalitat Valenciana. M.L is grateful for support under the ‘‘Programa de Recualificaci3n del Sistema Universitario Espa3ol para 2021-2023’’, (funded by ‘‘Instrumento Europeo de Recuperaci3n (Next Generation EU) en el marco del Plan de Recuperaci3n, Transformaci3n y Resiliencia de Espa3a’’, a trav3s del Ministerio de Universidades.

References

- [1] G. Wang, X. Wen, J. Wen, Y. Liu, Quasi-One-Dimensional Periodic Structure with Locally Resonant Band Gap, *Journal of Applied Mechanics* 73 (1) (2005) 167–170. arXiv:<https://asmigitalcollection.asme.org/appliedmechanics/article-pdf/73/1/167/doi:10.1115/1.2061947>. URL <https://doi.org/10.1115/1.2061947>
- [2] E. M. Jr., J. Dos Santos, Flexural wave band gaps in multi-resonator elastic metamaterial timoshenko beams, *Wave Motion* 91 (2019) 102391. doi:<https://doi.org/10.1016/j.wavemoti.2019.102391>. URL <https://www.sciencedirect.com/science/article/pii/S0165212519302756>

- [3] Z. Wang, P. Zhang, Y. Zhang, Locally resonant band gaps in flexural vibrations of a timoshenko beam with periodically attached multioscillators, *Mathematical Problems in Engineering* 2013 (Art. ID146975).
- [4] Y. Xiao, J. Wen, X. Wen, Broadband locally resonant beams containing multiple periodic arrays of attached resonators, *Physics Letters A* 376 (16) (2012) 1384–1390. doi:<https://doi.org/10.1016/j.physleta.2012.02.059>. URL <https://www.sciencedirect.com/science/article/pii/S037596011200254X>
- [5] Y. Xiao, J. Wen, D. Yu, X. Wen, Flexural wave propagation in beams with periodically attached vibration absorbers: Band-gap behavior and applications, *Journal of Sound and Vibration* 332 (4) (2013) 867–893. doi:<https://doi.org/10.1016/j.jsv.2012.09.035>. URL <https://www.sciencedirect.com/science/article/pii/S0022460X12007596>
- [6] R. Wiltshaw, J. M. De Ponti, R. V. Craster, Analytical solutions for Bloch waves in resonant phononic crystals: deep-subwavelength energy splitting and mode steering between topologically protected interfacial and edge states, *The Quarterly Journal of Mechanics and Applied Mathematics* 76 (2) (2023) 163–209.
- [7] F. Monticone, A. Alù, Metamaterial, plasmonic and nanophotonic devices, *Reports on Progress in Physics* 80 (3) (2017) 036401.
- [8] A. Ali, A. Mitra, B. Aïssa, Metamaterials and metasurfaces: A review from the perspectives of materials, mechanisms and advanced metadevices, *Nanomaterials* 12 (6) (2022) 1027.
- [9] S. A. Cummer, J. Christensen, A. Alù, Controlling sound with acoustic metamaterials, *Nature Reviews Materials* 1 (3) (2016) 1–13.
- [10] S. Brùlé, S. Enoch, S. Guenneau, Emergence of seismic metamaterials: Current state and future perspectives, *Physics Letters A* 384 (1) (2020) 126034.
- [11] Muhammad, C. W. Lim, From photonic crystals to seismic metamaterials: A review via phononic crystals and acoustic metamaterials, *Archives of Computational Methods in Engineering* 29 (2) (2022) 1137–1198.
- [12] A. O. Krushynska, D. Torrent, A. M. Aragón, R. Ardito, O. R. Bilal, B. Bonello, F. Bosia, Y. Chen, J. Christensen, A. Colombi, et al., Emerging topics in nanophononics and elastic, acoustic, and mechanical metamaterials: an overview, *Nanophotonics* 12 (4) (2023) 659–686.
- [13] Z. Chen, B. Guo, Y. Yang, C. Cheng, Metamaterials-based enhanced energy harvesting: A review, *Physica B: Condensed Matter* 438 (2014) 1–8.
- [14] G. J. Chaplain, J. M. De Ponti, G. Aguzzi, A. Colombi, R. V. Craster, Topological rainbow trapping for elastic energy harvesting in graded Su-Schrieffer-Heeger systems, *Physical Review Applied* 14 (5) (2020) 054035.
- [15] J. M. De Ponti, A. Colombi, R. Ardito, F. Braghin, A. Corigliano, R. V. Craster, Graded elastic metasurface for enhanced energy harvesting, *New Journal of Physics* 22 (1) (2020) 013013.
- [16] J. M. De Ponti, et al., *Graded elastic metamaterials for energy harvesting*, Springer, 2021.
- [17] A. Colombi, P. Roux, S. Guenneau, P. Gueguen, R. V. Craster, Forests as a natural seismic metamaterial: Rayleigh wave bandgaps induced by local resonances, *Scientific reports* 6 (1) (2016) 19238.
- [18] A. Colombi, D. Colquitt, P. Roux, S. Guenneau, R. V. Craster, A seismic metamaterial: The resonant metawedge, *Scientific reports* 6 (1) (2016) 27717.
- [19] M. Lott, P. Roux, S. Garambois, P. Guéguen, A. Colombi, Evidence of metamaterial physics at the geophysics scale: the METAFORÉT experiment, *Geophysical Journal International* 220 (2) (2020) 1330–1339.
- [20] D. Mu, H. Shu, L. Zhao, S. An, A review of research on seismic metamaterials, *Advanced Engineering Materials* 22 (4) (2020) 1901148.
- [21] A. Yakovleva, I. Movchan, D. Misseroni, N. Pugno, A. Movchan, Multi-physics of dynamic elastic metamaterials and earthquake systems, *Frontiers in Materials* 7 (2021) 620701.
- [22] V. G. Maz'ya, A. B. Movchan, M. J. Nieves, Mesoscale asymptotic approximations in the dynamics of solids with defects, *Journal of Mathematical Sciences* 268 (4) (2022) 443–457. doi:[10.1007/s10958-022-06214-y](https://doi.org/10.1007/s10958-022-06214-y).
- [23] M. J. Nieves, A. B. Movchan, Meso-scale method of asymptotic analysis of elastic vibrations in periodic and non-periodic multi-structures, *The Quarterly Journal of Mechanics and Applied Mathematics* 75 (3) (2022) 171–214. arXiv:<https://academic.oup.com/qjmam/article-pdf/75/3/171/45512028/hbac011.pdf>, doi:[10.1093/qjmam/hbac011](https://doi.org/10.1093/qjmam/hbac011).
- [24] M. J. Nieves, A. B. Movchan, Asymptotic theory of generalised rayleigh beams and the dynamic coupling, in: H. Altenbach, D. Prikazchikov, A. Nobili (Eds.), *Mechanics of High-Contrast Elastic Solids*, Springer International Publishing, Cham, 2023, pp. 173–200.
- [25] D. Torrent, J. Sánchez-Dehesa, Acoustic analogue of graphene: Observation of dirac cones in acoustic surface waves, *Phys. Rev. Lett.* 108 (2012) 174301. doi:[10.1103/PhysRevLett.108.174301](https://doi.org/10.1103/PhysRevLett.108.174301). URL <https://link.aps.org/doi/10.1103/PhysRevLett.108.174301>
- [26] R. Wiltshaw, R. V. Craster, M. P. Makwana, Asymptotic approximations for bloch waves and topological mode steering in a planar array of resonators, *Wave Motion* 99 (2020) 102662. doi:<https://doi.org/10.1016/j.wavemoti.2020.102662>. URL <https://www.sciencedirect.com/science/article/pii/S0165212520302924>
- [27] V. G. Maz'ya, A. B. Movchan, M. J. Nieves, Eigenvalue problem in a solid with many inclusions: Asymptotic analysis, *Multiscale Modeling & Simulation* 15 (2) (2017) 1003–1047. arXiv:<https://doi.org/10.1137/16M1079348>, doi:[10.1137/16M1079348](https://doi.org/10.1137/16M1079348). URL <https://doi.org/10.1137/16M1079348>
- [28] M. Nieves, G. Carta, I. Jones, A. Movchan, N. Movchan, Vibrations and elastic waves in chiral multi-structures, *Journal of the Mechanics and Physics of Solids* 121 (2018) 387–408. doi:<https://doi.org/10.1016/j.jmps.2018.07.020>. URL <https://www.sciencedirect.com/science/article/pii/S0022509618303570>
- [29] C. Sugino, Y. Xia, S. Leadenham, M. Ruzzene, A. Erturk, A general theory for bandgap estimation in locally resonant metastructures, *Journal of Sound and Vibration* 406 (2017) 104–123. doi:<https://doi.org/10.1016/j.jsv.2017.06.004>. URL <https://www.sciencedirect.com/science/article/pii/S0022460X17304704>

- [30] A. J. Croxford, P. D. Wilcox, B. W. Drinkwater, G. Konstantinidis, Strategies for guided-wave structural health monitoring, *Proceedings of the Royal Society A: Mathematical, Physical and Engineering Sciences* 463 (2087) (2007) 2961–2981.
- [31] J.-S. Wu, H.-M. Chou, Free vibration analysis of a cantilever beam carrying any number of elastically mounted point masses with the analytical method, *Journal of Sound and Vibration* 213 (2) (1998) 317–332. doi:<https://doi.org/10.1006/jsvi.1997.1501>. URL <https://www.sciencedirect.com/science/article/pii/S0022460X97915017>
- [32] M. Brennan, Control of flexural waves on a beam using a tunable vibration neutraliser, *Journal of Sound and Vibration* 222 (3) (1999) 389–407. doi:<https://doi.org/10.1006/jsvi.1998.2031>. URL <https://www.sciencedirect.com/science/article/pii/S0022460X98920314>
- [33] S.-K. Lee, B. Mace, M. Brennan, Wave propagation, reflection and transmission in non-uniform one-dimensional waveguides, *Journal of Sound and Vibration* 304 (1) (2007) 31–49. doi:<https://doi.org/10.1016/j.jsv.2007.01.039>. URL <https://www.sciencedirect.com/science/article/pii/S0022460X07001137>
- [34] C. Tan, B. Kang, Wave reflection and transmission in an axially strained, rotating timoshenko shaft, *Journal of Sound and Vibration* 213 (3) (1998) 483–510. doi:<https://doi.org/10.1006/jsvi.1998.1517>. URL <https://www.sciencedirect.com/science/article/pii/S0022460X98915176>
- [35] J. W. Lee, J. Y. Lee, Free vibration analysis using the transfer-matrix method on a tapered beam, *Computers & Structures* 164 (2016) 75–82. doi:<https://doi.org/10.1016/j.compstruc.2015.11.007>. URL <https://www.sciencedirect.com/science/article/pii/S0045794915003041>
- [36] V. Adámek, F. Vales, Analytical solution for a heterogeneous timoshenko beam subjected to an arbitrary dynamic transverse load, *European Journal of Mechanics - A/Solids* 49 (2015) 373–381. doi:<https://doi.org/10.1016/j.euromechsol.2014.07.016>. URL <https://www.sciencedirect.com/science/article/pii/S0997753814001211>
- [37] H. Aya, R. Cano, H. Zhevandrov, Scattering and embedded trapped modes for an infinite nonhomogeneous timoshenko beam, *J Eng Math* 77 (2012) 87–104.
- [38] K. Zhang, X. Yan, Multi-cracks identification method for cantilever beam structure with variable cross-sections based on measured natural frequencies, *Journal of Sound and Vibration* 387 (2017) 53–65. doi:<https://doi.org/10.1016/j.jsv.2016.09.028>. URL <https://www.sciencedirect.com/science/article/pii/S0022460X16304953>
- [39] P. Wang, F. Casadei, S. H. Kang, K. Bertoldi, Locally resonant band gaps in periodic beam lattices by tuning connectivity, *Physical Review B* 91 (2) (2015) 020103.
- [40] G. Aguzzi, C. Kanellopoulos, R. Wiltshaw, R. V. Craster, E. N. Chatzi, A. Colombi, Octet lattice-based plate for elastic wave control, *Scientific Reports* 12 (1) (2022) 1088. doi:[10.1038/s41598-022-04900-0](https://doi.org/10.1038/s41598-022-04900-0). URL <https://doi.org/10.1038/s41598-022-04900-0>
- [41] M. Krawczuk, W. M. Ostachowicz, A finite plate element for dynamic analysis of a cracked plate, *Computer methods in applied mechanics and engineering* 115 (1994) 67–78.
- [42] M. Krawczuk, W. M. Ostachowicz, a. Zak, Analysis of natural frequencies of delaminated composite beams based on finite element method, *Structural Engineering and Mechanics* 4 (3) (1996) 243–255.
- [43] M. Krawczuk, W. Ostachowicz, Spectral finite element and genetic algorithm for crack detection in cantilever rod., in: Holford, KM and Brandon, JA and DulieuBarton, JM and Gilchrist, MD and Worden, K (Ed.), *DAMAGE ASSESSMENT OF STRUCTURES*, Vol. 204-2 of KEY ENGINEERING MATERIALS, 2001, pp. 241–249, 4th International Conference on Damage Assessment of Structures (DAMAS 2001), CARDIFF, WALES, JUN 25-28, 2001.
- [44] M. Krawczuk, M. Palacz, W. Ostachowicz, The dynamic analysis of a cracked Timoshenko beam by the spectral element method, *Journal of Sound and Vibration* 264 (5) (2003) 1139–1153.
- [45] C. Yeung, C. T. Ng, Time-domain spectral finite element method for analysis of torsional guided waves scattering and mode conversion by a crack, *Mechanical Systems and Signal Processing* 128 (2019) 305–317. doi:<https://doi.org/10.1016/j.ymsp.2019.04.013>. URL <https://www.sciencedirect.com/science/article/pii/S0888327019302432>
- [46] M. Loghmani, M. R. Hairi Yazdi, An analytical method for free vibration of multi cracked and stepped nonlocal nanobeams based on wave propagation method, *Results in Physics* 11 (2018) 166–181. doi:<https://doi.org/10.1016/j.rinp.2018.08.046>. URL <https://www.sciencedirect.com/science/article/pii/S2211379718316188>
- [47] M. Loghmani, M. R. Hairi Yazdi, M. Nikkhab Bahrami, Longitudinal vibration analysis of nanorods with multiple discontinuities based on the transfer matrix method, *Microsystem Technologies* 24 (5) (2018) 2445–2461. doi:[10.1007/s00542-017-3619-y](https://doi.org/10.1007/s00542-017-3619-y). URL <https://doi.org/10.1007/s00542-017-3619-y>
- [48] J. F. Doyle, *Wave Propagation in Structures. Spectral Analysis Using Fast Discrete Fourier Transforms*, Springer (New York), 1997.
- [49] K. F. Graff, *Wave Motion in Elastic Solids*, DOVER PUBLICATIONS, 1999.
- [50] *Elastic Waves in Solids 1*, John Wiley & Sons, 2022.
- [51] M. Lázaro, R. Wiltshaw, R. V. Craster, L. M. García-Raffi, Analytical approximations for multiple scattering in one-dimensional waveguides with small inclusions, *ArXiv e-prints* (arxiv.org/abs/2405.02587).
- [52] M. Lázaro, R. Wiltshaw, R. V. Craster, V. Romero-García, Wave propagation in beams with multiple resonators: conditions for weak scattering and the born approximation, *ArXiv e-prints* ([arXiv:2410.00188](https://arxiv.org/abs/2410.00188)).
- [53] X. Rui, G. Wang, J. Zhang, *Transfer matrix method for multibody systems theory and applications*, John Wiley & Sons, 2019.
- [54] A. Sommerfeld, *Partial differential equations in physics*, Academic press, 1949.

	Rod	Euler-Bernoulli beam	Timoshenko beam
A	$\begin{bmatrix} 0 & 1/EA \\ -\rho A\omega^2 & 0 \end{bmatrix}$	$\begin{bmatrix} 0 & 1 & 0 & 0 \\ 0 & 0 & 0 & 1/EI_y \\ -\rho A\omega^2 & 0 & 0 & 0 \\ 0 & 0 & -1 & 0 \end{bmatrix}$	$\begin{bmatrix} 0 & 1 & 1/GA_z & 0 \\ 0 & 0 & 0 & 1/EI_y \\ -\rho A\omega^2 & 0 & 0 & 0 \\ 0 & -\rho I_y\omega^2 & -1 & 0 \end{bmatrix}$
λ	$\begin{bmatrix} \lambda_1 & 0 \\ 0 & \lambda_2 \end{bmatrix}$	$\begin{bmatrix} \lambda_1 & 0 & 0 & 0 \\ 0 & \lambda_2 & 0 & 0 \\ 0 & 0 & \lambda_3 & 0 \\ 0 & 0 & 0 & \lambda_4 \end{bmatrix}$	$\begin{bmatrix} \lambda_1 & 0 & 0 & 0 \\ 0 & \lambda_2 & 0 & 0 \\ 0 & 0 & \lambda_3 & 0 \\ 0 & 0 & 0 & \lambda_4 \end{bmatrix}$
\mathbf{u}_j	$\frac{1}{\sqrt{2}} \begin{Bmatrix} 1 \\ EA\lambda_j \end{Bmatrix}$	$\frac{1}{2} \begin{Bmatrix} 1 \\ \lambda_j \\ -\frac{\rho A\omega^2}{\lambda_j} \\ EI_y\lambda_j^2 \end{Bmatrix}$	$\frac{1}{\gamma_j} \begin{Bmatrix} 1 \\ \frac{\lambda_j^2 + \kappa_s^2}{\lambda_j} \\ -\frac{\rho A\omega^2}{\lambda_j} \\ EI_y(\lambda_j^2 + \kappa_s^2) \end{Bmatrix}$
\mathbf{v}_j	$\frac{1}{\sqrt{2}} \begin{Bmatrix} 1 \\ -\frac{\lambda_j}{EA\kappa_c^2} \end{Bmatrix}$	$\frac{1}{2} \begin{Bmatrix} 1 \\ 1/\lambda_j \\ -\frac{\lambda_j}{\rho A\omega^2} \\ 1/EI_y\lambda_j^2 \end{Bmatrix}$	$\frac{1}{\gamma_j} \begin{Bmatrix} 1 \\ \frac{\lambda_j}{\lambda_j^2 + r^2\kappa_f^4} \\ -\frac{\lambda_j}{\rho A\omega^2} \\ \frac{1}{EI_y(\lambda_j^2 + r^2\kappa_f^4)} \end{Bmatrix},$
λ_1	$-i\kappa_c$	$-i\kappa_f$	$-i\kappa_{fb}$
λ_2	$+i\kappa_c$	$-\kappa_f$	$-\kappa_{fs}$
λ_3	$-$	$+i\kappa_f$	$+i\kappa_{fb}$
λ_4	$-$	$+\kappa_f$	$+\kappa_{fs}$
	$\kappa_c = \omega \sqrt{\frac{\rho A}{EA}}$	$\kappa_f = \left(\omega^2 \frac{\rho A}{EI_y}\right)^{1/4}$	$\kappa_{fb} = \frac{\Omega}{r} \sqrt{\frac{1+\alpha^2}{2}} \sqrt{\eta + 1}$ $\kappa_{fs} = \frac{\Omega}{r} \sqrt{\frac{1+\alpha^2}{2}} \sqrt{\eta - 1}$ $\gamma_j = \sqrt{2 \left(1 + \frac{\lambda_j^2 + \kappa_s^2}{\lambda_j^2 + r^2\kappa_f^4}\right)}$

Table C.4: Wavemodes of some elastic 1D waveguides: a classical rod (compressional waves), a classical beam (flexural waves), a higher order beam (flexural and shear waves). Auxiliari parameters as α , η , Ω , r are given in Eq. (C.1)